ACCSCIENCE PUBLISHING

Eurasian Journal of Medicine and Oncology

ORIGINAL RESEARCH ARTICLE

Targeting the FN3K–Nrf2 axis: Discovery and pre-clinical evaluation of novel inhibitors for breast cancer therapy

Erica Alves, Gurupadayya Bannimath*, and Prabitha Prabhakaran

Department of Pharmaceutical Chemistry, JSS College of Pharmacy, JSS Academy of Higher Education & Research, Mysore, Karnataka, India

Abstract

Introduction: Fructosamine-3-kinase (FN3K), a deglycation enzyme implicated in redox regulation through the nuclear factor erythroid 2-related factor 2 (Nrf2) pathway, has emerged as a novel therapeutic target in breast cancer. Elevated FN3K activity enhances antioxidant defenses, promoting cancer cell survival and resistance to therapies. Pharmacological inhibition of FN3K may sensitize tumors to oxidative stress.
Objective: This study aimed to identify and validate potent FN3K inhibitors through structure-based virtual screening (SBVS) and *in vitro* evaluation in breast cancer models.
Methods: A homology-modeled FN3K structure was generated and validated using SWISS-MODEL, PROCHECK, and QMEAN. Compound libraries, including the Food and Drug Administration (FDA)-approved kinase inhibitors, World Health Organization (WHO) essential medicines, and anti-breast cancer agents, were screened using Schrödinger's Glide module. Top-ranked compounds were prioritized based on binding affinity, molecular interactions, absorption, distribution, metabolism, excretion, and toxicity (ADMET) profiling. *In vitro* validation in MCF-7, BT-474, T-47D, and Vero cell lines included MTT cytotoxicity assay and evaluation of FN3K and Nrf2 expression through quantitative PCR (qPCR) and Western blotting. Statistical analyses were performed to assess the significance of observed effects.
Results: Oxaliplatin, lansoprazole, and capivasertib exhibited strong binding affinities (Glide scores: –9.2 to –8.1 kcal/mol) and selective cytotoxicity in breast cancer cell lines ($IC_{50:}$ 90 – 110 µg/mL). qPCR analysis revealed >99% downregulation of FN3K, accompanied by significant suppression of Nrf2 in cancer cells. Minimal modulation was observed in Vero cells, indicating tumor selectivity. Western blotting further corroborated the downregulation of FN3K and Nrf2 at the protein level. Molecular dynamics (MD) simulations validated the binding stability of the lead small molecules, reinforcing their potential as effective inhibitors.
Conclusion: The integrated *in silico* and *in vitro* analysis supports FN3K as a viable therapeutic target in breast cancer. Oxaliplatin, lansoprazole, and capivasertib demonstrated strong FN3K inhibition and modulation of tumor redox homeostasis, suggesting their potential for further pre-clinical development as novel anti-cancer agents targeting metabolic adaptability.

Keywords: Breast neoplasms; Fructosamine-3-kinase; Nuclear factor erythroid 2-related factor 2 protein; Oxidative stress; Antineoplastic agents

***Corresponding author:**
Gurupadayya Bannimath
(bmgurupadayya@jssuni.edu.in)

Citation: Alves E, Bannimath G, Prabhakaran P. Targeting the FN3K–Nrf2 axis: Discovery and pre-clinical evaluation of novel inhibitors for breast cancer therapy. *Eurasian J Med Oncol*. 2025;9(3):197-225. doi: 10.36922/EJMO025150114

Received: April 13, 2025

Revised: May 17, 2025

Accepted: June 4, 2025

Published online: July 28, 2025

1. Introduction

Breast cancer persists as a predominant contributor to global cancer-related mortality, with the efficacy of present therapeutic modalities often constrained by systemic toxicities and the progressive development of multidrug resistance.[1] Recent global statistics indicate that, in 2022, breast cancer was diagnosed in approximately 2.3 million women worldwide, leading to more than 670,000 reported deaths.[1] Although incidence rates are higher in high-income countries, mortality remains disproportionately elevated in low-resource settings due to delayed diagnosis and limited access to effective treatment options. The complexity of breast cancer, encompassing diverse molecular subtypes, presents significant therapeutic challenges.[1]

Resistance to chemotherapeutic agents and targeted therapies continues to undermine treatment efficacy, underscoring the urgent need for novel therapeutic strategies. Emerging evidence underscores metabolic reprogramming as a critical driver of cancer progression and therapeutic resistance.[2] To sustain uncontrolled growth and adapt to the tumor microenvironment, cancer cells exhibit marked metabolic adaptability driven by alterations in glycolysis, glutamine utilization, lipid processing, and mitochondrial respiration.[2] Targeting key metabolic enzymes within these reprogrammed pathways – such as hexokinase II, glutaminase, and fatty acid synthase – has emerged as a promising therapeutic strategy, offering selectivity by exploiting cancer-specific metabolic dependencies.[2] However, the dynamic nature of metabolic adaptation highlights the need for combinatorial approaches and robust biomarkers to improve therapeutic efficacy.[2]

Fructosamine-3-kinase (FN3K) is a deglycating enzyme that catalyzes the phosphorylation of fructosamine adducts on glycated proteins, thereby promoting their elimination and aiding in protein quality control and repair. This enzymatic activity plays a crucial role in mitigating cellular damage associated with non-enzymatic glycation, oxidative stress, and metabolic dysregulation. A marked reduction in FN3K activity has been observed in breast cancer tissues compared to adjacent normal tissues, indicating its potential involvement in tumor progression and diminished defense against advanced glycation end products (AGEs).[3] Beyond its role in protein repair through deglycation, FN3K has been implicated in cancer progression by contributing to the stabilization of nuclear factor erythroid 2-related factor 2 (Nrf2), a key transcription factor governing antioxidant defense mechanisms. This stabilization enhances Nrf2-mediated transcription of cytoprotective genes, thereby promoting cancer cell proliferation, survival, and resistance to therapy. FN3K facilitates metabolic adaptability in cancer cells by alleviating oxidative stress and maintaining redox homeostasis, thereby underscoring its potential as an emerging therapeutic target in breast cancer.[4] FN3K modulates the activity of redox-sensitive transcription factors, such as Nrf2 by catalyzing the deglycation of essential lysine and arginine residues critical for transcriptional activation. Glycation of Nrf2 impairs its stability, nuclear translocation, and interaction with small musculoaponeurotic fibrosarcoma (sMAF) proteins, thereby attenuating its antioxidant transcriptional program. Conversely, FN3K overexpression maintains Nrf2 in a functional state, promoting redox homeostasis and facilitating tumor cell survival under oxidative stress. Elevated FN3K activity has been associated with enhanced Nrf2 signaling and poor prognosis in multiple cancer types, including breast cancer, underscoring its role in disease progression and therapy resistance.[5]

Using structure-based virtual screening (SBVS) combined with molecular docking, Beeraka *et al.*[5] reported that multiple anti-cancer compounds – including tyrosine kinase inhibitors, hormonal modulators, and immunosuppressants – exhibited strong modulatory effects on FN3K activity.[6] Beeraka *et al.*[5] also identified several anti-cancer agents – including gefitinib, sorafenib, neratinib, tamoxifen citrate, and cyclosporine A – as potent modulators of FN3K through SBVS and molecular docking approaches.[6] A separate study demonstrated a strong positive correlation between FN3K levels and Nrf2-target antioxidant gene expression signatures, implicating FN3K in sustaining redox homeostasis through Nrf2 pathway protection. Notably, elevated FN3K expression has been correlated with decreased disease-specific survival, indicating its potential relevance as a prognostic biomarker in breast cancer.[7] Yousefi *et al.*[2] conducted a comparative enzymatic analysis of FN3K activity in paired breast tumor and adjacent normal tissues, revealing a significant reduction in FN3K activity within tumor samples. This reduction may compromise cellular deglycation efficiency, leading to the accumulation of AGEs, which can disrupt protein function, elevate oxidative stress, and facilitate malignant transformation by driving metabolic reprogramming. These observations highlight FN3K as a potential regulator of metabolic pathways involved in the pathogenesis of breast cancer.[3] FN3K mediates a distinctive intracellular deglycation process by phosphorylating fructosamine adducts at the third carbon of the deoxyfructose ring, thereby promoting their spontaneous breakdown and restoring free amino groups. This enzymatic correction limits the formation of stable AGEs, which are associated with persistent oxidative stress and inflammation – key pathophysiological factors in cancer initiation and progression.[8]

Pharmacological inhibition of FN3K represents a novel therapeutic strategy to disrupt Nrf2-mediated antioxidant defense mechanisms that enable cancer cell survival, proliferation, and resistance to therapy. Inhibiting FN3K may preserve Nrf2 in its glycated and transcriptionally inactive form, thereby increasing cancer cell susceptibility to oxidative stress and potentially augmenting the therapeutic effectiveness of standard interventions, such as chemotherapy and radiotherapy. However, despite its therapeutic promise, FN3K remains an underexplored target in oncology, with limited progress in the identification and development of potent, selective small molecule inhibitors.[4] The pursuit of novel anti-cancer agents has been significantly accelerated by the emergence of SBVS, a pivotal component of computer-aided drug discovery. SBVS enables the high-throughput computational screening of large chemical libraries against well-defined biological targets, leveraging structural insights to identify potential lead compounds with enhanced specificity and binding affinity. Compared to traditional high-throughput screening methods, virtual screening (VS) offers substantial reductions in time, cost, and resource expenditure, while improving hit rates through rational design strategies. Moreover, recent advancements in docking algorithms, scoring functions, and ensemble-based receptor modeling have further enhanced the accuracy and success rate of SBVS in anti-cancer drug discovery.[9] In addition to its role in Nrf2 regulation, recent advances have clarified that FN3K plays a multifaceted role in cancer progression. FN3K deglycates key lysine and arginine residues on Nrf2, enhancing its nuclear stability and enabling antioxidant response element (ARE)-driven transcription of antioxidant and cytoprotective genes, such as heme oxygenase-1 (HO-1), NAD(P)H quinone dehydrogenase 1 (NQO1), and thioredoxin reductase 1 (TXNRD1), which collectively contribute to redox homeostasis, chemoresistance, and tumor survival.[3,4,10] Conversely, inhibiting FN3K impairs Nrf2's interaction with sMAF proteins, reduces nuclear translocation, and suppresses downstream antioxidant responses, thereby sensitizing cancer cells to oxidative stress.[4,5] Moreover, FN3K modulates broader signaling networks through glycation stress; the AGE and the receptor for AGE (AGE-RAGE) systems stimulate oncogenic cascades, including phosphoinositide 3-kinase/protein kinase B (PI3K/Akt), mitogen-activated protein kinase (MAPK), and Janus kinase/signal transducer and activator of transcription 3 (JAK/STAT3), promoting epithelial–mesenchymal transition, angiogenesis, and immune evasion.[3,10] Dual inhibition strategies (e.g., oxaliplatin + brusatol) have demonstrated enhanced reactive oxygen species (ROS)-mediated apoptosis, reduced migration and clonogenicity, and dose-sparing cytotoxic effects.[11] FN3K is also implicated in mitochondrial regulation, glutathione metabolism, and extracellular matrix (ECM) remodeling – hallmarks of tumor metabolic adaptation.[3] These findings position FN3K as a central modulator of cancer redox biology and metabolism, offering therapeutic leverage beyond Nrf2 regulation.

The present study investigates the therapeutic relevance of FN3K inhibition in breast cancer, aiming to evaluate its potential to overcome drug resistance and enhance treatment outcomes through an integrated *in silico*, *in vitro*, and *in vivo* approach. This study utilizes three curated and pharmacologically validated compound databases as the primary source for VS. The first database comprises the Food and Drug Administration (FDA)-approved kinase inhibitors, which are designed to modulate aberrant kinase signaling – a hallmark of various malignancies. Given the central role of protein kinases in regulating key cellular processes and their frequent dysregulation in cancer, this class of therapeutics represents one of the most extensively targeted mechanisms in oncology. As of 2024, 80 small molecule kinase inhibitors have received FDA approval, of which 69 are indicated for cancer treatment, underscoring their clinical relevance in oncology.[12] The second compound library was sourced from the World Health Organization (WHO) Model List of Essential Medicines, a globally endorsed collection of drugs selected based on their proven efficacy, safety, affordability, and significance to public health. These compounds are clinically relevant, possess well-documented safety profiles, and are widely applicable across diverse therapeutic settings.[13] The third dataset comprises FDA-approved therapeutics used in breast cancer management, including agents that act on various molecular targets, such as estrogen and progesterone receptors, human epidermal growth factor receptor 2 (HER2), and key regulators of the cell cycle. These drugs constitute the cornerstone of present treatment protocols and may present repurposing opportunities if found to inhibit FN3K. Such dual-function compounds hold promise in attenuating both breast cancer progression and FN3K-driven metabolic adaptability.[14]

This study employed SBVS to identify potential small molecule binders with strong affinity toward the FN3K enzyme. SBVS involves molecular docking techniques that simulate the interaction of candidate compounds within the enzyme's active site, assessing their steric and electrostatic compatibility. To predict binding affinities and rank potential candidates, a combination of scoring functions – spanning empirical methods, force field-based approaches, and knowledge-driven models – was utilized to evaluate the stability of ligand-enzyme

interactions. This approach facilitates rational drug design by streamlining lead identification from extensive chemical libraries, minimizing experimental workload, and improving hit enrichment.[15] Lead molecule selection for therapeutic development represents a critical phase in the drug discovery pipeline, necessitating the validation of computational predictions through robust experimental assays. Lead candidates were strategically selected from the initial SBVS hits by evaluating their predicted binding strength and structural compatibility with the FN3K enzyme. These candidates were then subjected to biological evaluation to confirm their ability to inhibit FN3K enzymatic activity.[16] The overarching aim was to identify potent inhibitors capable of suppressing FN3K function, thereby offering potential therapeutic benefit in the context of breast cancer management.

To confirm computational findings and evaluate the biological significance of the selected FN3K inhibitors, *in vitro* assays were performed using quantitative PCR (qPCR) and Western blotting. These assays were utilized to investigate the expression patterns of FN3K and the redox-responsive transcription factor Nrf2, a key regulator of cellular antioxidant defenses and chemoresistance. Earlier research has shown that abnormal elevation of Nrf2 expression promotes tumor cell survival in oxidative environments, while its suppression increases cancer cell vulnerability to chemotherapeutic agents. This study also investigated the relationship between FN3K and Nrf2 expression across various breast cancer subtypes, underscoring their potential co-regulatory involvement in redox homeostasis and tumor progression.[7,17] By identifying compounds that selectively inhibit FN3K activity, we aimed to uncover novel therapeutic agents with potential applications in breast cancer management. FN3K plays a pivotal role in cancer progression by stabilizing and enhancing the oncogenic potential of Nrf2 through deglycation, thereby enabling sustained activation of antioxidant and survival pathways in tumor cells. Therefore, targeting FN3K offers a promising therapeutic strategy to attenuate aberrant Nrf2 signaling, overcome drug resistance, and sensitize cancer cells to oxidative stress. The identification of promising lead compounds exhibiting strong FN3K-inhibitory activity lays the groundwork for the rational design of novel anti-cancer strategies, particularly in breast cancer, where FN3K overexpression has been linked to unfavorable clinical outcomes. Taken together, this work illustrates the effectiveness of combining computational approaches, such as VS, with *in vitro* validation to accelerate the identification of targeted therapeutic candidates. The FN3K–Nrf2 signaling axis emerges as a novel and relatively unexplored target in cancer research, with FN3K inhibition offering promising prospects for advancing personalized treatment modalities.[4]

2. Materials and methods

2.1. SBVS

2.1.1. Materials

2.1.1.1. Software

Schrödinger Maestro (Schrödinger, LLC, USA) was used as a comprehensive molecular modeling environment for preparing, visualizing, and analyzing molecular structures.[18] For molecular docking, the Schrödinger Glide module within Maestro, was employed, as it is widely used for VS and drug discovery.[19]

2.1.1.2. Datasets

Kinase inhibitors approved by the FDA are integral components of cancer treatment due to their targeted mechanisms of action.[12] The WHO Model Essential Medicines list comprises pharmacological agents recognized for their clinical efficacy, safety profile, and widespread use in medical practice, as endorsed by the WHO.[13] In addition, FDA-approved anti-breast cancer agents represent a curated list of approved drugs specifically targeting breast cancer, offering potential repositioning opportunities.[14]

2.1.1.3. Computational resources

A high-performance computing cluster or a powerful workstation with sufficient memory and processing power was used to handle molecular simulations and docking calculations.[20]

2.1.1.4. Protein and ligand data

The three-dimensional (3D) structure of the target protein was generated through comparative or homology modeling to enable precise molecular docking and reliable assessment of ligand–protein interactions.[21] Ligand datasets were obtained from reputable sources, such as DrugBank, PubChem, and the FDA, providing well-characterized small molecules for VS.[12-14]

2.1.2. Methods

2.1.2.1. Construction of the 3D structure of the protein

The 3D structure of human FN3K was constructed through a systematic multistep process. First, the amino acid sequence of human FN3K, consisting of 309 residues and indexed under UniProt ID Q9H479, was retrieved from the UniProt database.[22] Phylogenetic similarities among FN3K sequences were then assessed using Clustal Omega, a robust tool for multiple sequence alignment.[23] For homology

modeling, a suitable structural template for FN3K was generated using SWISS-MODEL, an automated web-based tool for protein structure prediction based on sequence homology.[24] The preliminary FN3K model was further refined using the GalaxyWEB server, a platform providing specialized tools for protein structure optimization.[25] To ensure reliability and precision, the refined FN3K model underwent rigorous validation through various analytical techniques. Ramachandran plot analysis was performed to evaluate the ϕ (phi) and ψ (psi) dihedral angles of amino acid residues, confirming their placement within sterically favorable regions of the protein structure.[26] PROCHECK, accessed through the SAVES server at UCLA (https://saves.mbi.ucla.edu/), was used to assess the stereochemical quality and geometric parameters of the model.[27] In addition, the Global Model Quality Estimation (GMQE) score provided by SWISS-MODEL was considered to gauge the predicted reliability of the generated model.[28] Finally, Qualitative Model Energy Analysis (QMEAN) values were examined to estimate overall model quality based on multiple scoring functions.[29,30]

2.1.2.2. Protein preparation

To prepare the protein structure constructed through homology modeling, the generated model was imported into Maestro. Using the Protein Preparation Wizard within Maestro, several essential steps were undertaken to refine the homology-modeled protein structures.[31]

2.1.2.3. Preparation of ligand libraries

In preparing the ligand libraries, ligand datasets were curated from databases, such as DrugBank, PubChem, and the FDA.[12,32,33] The selected ligand structures were then imported into Maestro, where the LigPrep tool was used to generate 3D conformations from the 2D structures.[34]

2.1.2.4. Identification of potential binding sites

Potential ligand-binding regions on the modeled FN3K structure were predicted using the SiteMap module integrated within the Maestro software suite. SiteMap is an advanced computational tool designed to detect and characterize binding pockets and cavities within a protein structure.[35]

2.1.2.5. Preparation of the receptor grid

Following the identification of potential binding sites using SiteMap, the next step involved the preparation of the receptor grid. The receptor grid generation tool in Maestro was used for this purpose.[34]

2.1.2.6. Docking

The molecular docking setup was initiated by selecting the standard-precision (SP) mode within Glide. Glide is a molecular docking tool that predicts the binding affinity and orientation of ligands within a receptor binding site.[36]

2.1.2.7. Post-docking analysis

The docking results generated by Glide were analyzed to identify hit molecules based on binding affinity (Glide score) and key interactions with the FN3K active site. Binding conformations were evaluated for key molecular interactions, including hydrogen bonding, hydrophobic contacts, and π-π stacking.[37]

2.1.2.8. Absorption, distribution, metabolism, excretion, and toxicity (ADMET) screening

The shortlisted hit molecules from the post-docking analysis underwent the ADMET screening to assess their drug-like properties and safety profiles. This filtering step ensured the identification of compounds with both high binding affinity and desirable pharmacokinetic properties for further consideration.[38]

2.2. In vitro screening studies

2.2.1. In vitro cytotoxicity evaluation

2.2.1.1. Cell lines and culture conditions

The cytotoxicity of the selected compounds was assessed using human breast cancer cell lines – MCF-7, T47D, and BT-474 – as well as non-malignant Vero cells. All cell lines were cultured in Dulbecco's Modified Eagle's Medium (DMEM) supplemented with 10% fetal calf serum (FCS), 100 U/mL penicillin, 100 µg/mL streptomycin, and 50 µg/mL kanamycin. Cells were maintained at 37°C in a humidified incubator containing 5% CO_2 until approximately 70% confluency was achieved.[39]

2.2.1.2. 3-[4,5-dimethylthiazol-2-yl]-2,5-diphenyl tetrazolium bromide (MTT) assay

The cytotoxic effects of 1-deoxy-morpholino-D-fructose (1-DMF), ritonavir, amiloride, lansoprazole, capivasertib, and oxaliplatin were investigated using the MTT assay, following the ISO 10993-5:2009 guidelines for *in vitro* cytotoxicity assessment.[40] Cells were dispensed into 96-well plates at a density of 1×10^4 cells per well and incubated for 24 h to allow adherence under standard conditions. Thereafter, cells were treated in triplicates with a range of compound concentrations (12.5 – 200 µg/mL), tailored to individual solubility and bioactivity profiles, and incubated for an additional 24-h period.[41]

Post-treatment, 20 µL of MTT solution at 5 mg/mL, prepared in phosphate-buffered saline (PBS), was added to each well, followed by a 4-h incubation at 37°C to allow for formazan crystal formation.[40] The resulting crystals were solubilized using 100 µL of isopropanol containing 0.04N

hydrochloric acid (HCl). Absorbance was then recorded at 570 nm using a microplate spectrophotometer. Untreated cells served as the negative control for determining relative cell viability.[41]

2.2.2. qPCR evaluation

2.2.2.1. Cell culture and treatment

MCF-7, BT-474, and T-47D human breast cancer cell lines, along with non-malignant Vero cells, were cultured as adherent monolayers in 25 cm^2 tissue culture flasks. The cells were maintained in DMEM supplemented with 10% FCS and antibiotics, including penicillin and streptomycin, under standard incubation conditions at 37°C with 5% CO_2 and high humidity. Cultures were allowed to grow until approximately 70% confluency was achieved.[42] Cells were gently rinsed with 1× PBS and subsequently detached using 0.2% trypsin-EDTA at a volume of 200 µL per flask for 5 min at room temperature. The dissociated cells were then seeded into 6-well plates at a volume of 1.0 mL per well. The cells were allowed to adhere and stabilize for 48 h before treatment.

2.2.2.2. Total RNA isolation

Cell pellets were resuspended in TRIzol reagent and mixed thoroughly, followed by the addition of 300 µL chloroform to each sample.[43] After brief vortexing, the samples were incubated at room temperature for 15 min. Phase separation was carried out by centrifugation at 14,000 rpm for 10 min at 4°C, and the resulting aqueous phase was carefully transferred to a new microcentrifuge tube. An equal volume of isopropanol was then added, mixed gently, and incubated at room temperature for 5 min to precipitate RNA, followed by centrifugation under the same conditions. The RNA pellet was washed with 70% ethanol, air-dried, and reconstituted in 100 µL of diethyl pyrocarbonate (DEPC)-treated water. RNA purity and concentration were then determined spectrophotometrically by measuring absorbance at 260 nm.[44]

2.2.2.3. Complementary DNA (cDNA) synthesis

First-strand cDNA synthesis was performed using 5 µg of total RNA according to standardized reverse transcription protocols. The reaction mixture was prepared by combining 2 µL of total RNA (~5 µg), 2 µL of random hexamer or oligo(dT) primers, 2 µL of 10 mM dNTP mix, and 4 µL of DEPC-treated water. This mixture was heated at 65°C for 2 min to denature secondary structures and then allowed to equilibrate to room temperature. Next, 2 µL of 10× reverse transcription buffer, 4 µL of 25 mM $MgCl_2$, 2 µL of 0.1 M DTT, and 1 µL of RNase inhibitor were added. The mixture was pre-incubated at 25°C for 2 min, after which 1 µL of SuperScript II Reverse Transcriptase (Invitrogen, USA) was added. The enzymatic reaction was carried out through a thermal program consisting of 10 min at 25°C, 90 min at 42°C, and 15 min at 70°C to inactivate the enzyme. After a brief centrifugation step, 1 µL of RNase H was added to degrade the RNA template, followed by incubation at 37°C for 30 min. The synthesized cDNA was stored at −20°C until further use.

2.2.2.4. qPCR Analysis

The cDNA was diluted 1:1 with DEPC-treated water before amplification.[45] Each 10 µL qPCR reaction consisted of 1 µL of diluted cDNA, 1 µL of gene-specific primer mix (forward and reverse), 5 µL of SYBR® Green Supermix (Bio-Rad; Cat. No. 172-5270, USA), and nuclease-free Milli-Q water to reach the final volume.

qPCR was conducted using the QuantStudio 5 Real-Time PCR System (Applied Biosystems, USA) under a thermal protocol comprising 40 amplification cycles. Cycle threshold (Ct) values were recorded for each target gene, and relative gene expression levels were quantified using the ΔΔCt method. This approach ensures precise normalization and reliable detection of low-abundance transcripts, minimizing technical variability.[46,47]

2.2.2.5. Primer sequences

The specific primer sequences used for the amplification of FN3K, Nrf2, and ACTB (Beta actin) genes were summarized in Table 1.

2.2.3. Western blot analysis

2.2.3.1. Cell culture and treatment

MCF-7, BT-474, and T-47D human breast cancer cell lines, along with non-malignant Vero cells, were cultured as adherent monolayers in 25 cm^2 tissue culture flasks. The cells were maintained in DMEM supplemented with 10% FCS, penicillin, and streptomycin under standard incubation conditions at 37°C with 5% CO_2 in a humidified atmosphere, until approximately 70% confluency was reached.[7]

Cells were then rinsed with 1× PBS and detached by treating with 0.2% trypsin-EDTA at a volume of 200 µL per flask for 5 min at room temperature. The detached cells were resuspended in complete DMEM containing 10% FCS and antibiotics, and subsequently seeded into 6-well plates at a volume of 1.0 mL per well. After a 48-h adherence period, the cells were treated for 24 h with selected compounds – amiloride, capivasertib, ritonavir, oxaliplatin, lansoprazole, and 1-DMF.

Following treatment, cells were harvested, washed once with 1× PBS, and resuspended in 500 µL of 1× PBS. To each

Table 1. Primer sequences used for amplification of *FN3K, Nrf2*, and *ACTB* genes

Gene	Forward primer (5' → 3')	Reverse primer (5' → 3')	Reference
FN3K	GGGTGCTGAGCCTCAGTATGTGG	CCTTCTCAATGAGGTCCAGCTGC	Designed using Primer-BLAST
Nrf2	CATCGAGAGCCCAGTCTTCATTTGC	GCTTGTCATTTTCAATATTAAGAC	Designed using Primer-BLAST
ACTB	CATGCCATCCTGCGTCTGGACCTG	GTCCAGGGCGACGTAGCACAGC	Housekeeping gene

sample, 500 µL of 3× Laemmli sample buffer (50 mM Tris-HCl, pH 6.8; 100 mM DTT; 7% SDS; 0.1% bromophenol blue; and 10% glycerol) was added. The mixture was then heat-denatured at 95°C for 5 min in preparation for sodium dodecyl-sulfate polyacrylamide gel electrophoresis (SDS-PAGE).

2.2.3.2. SDS-PAGE

SDS-PAGE was carried out following the Laemmli protocol using a vertical gel electrophoresis system with a discontinuous buffer setup. The resolving gel was prepared with 8% acrylamide in 0.375 M Tris-HCl buffer (pH 8.8) containing 0.1% SDS, while the stacking gel comprised 5% acrylamide in 0.125 M Tris-HCl buffer (pH 6.8) with 0.1% SDS. Polymerization was initiated by the addition of tetramethylethylenediamine (TEMED) and ammonium persulfate (APS).

Protein samples were loaded into the wells, and electrophoretic separation was conducted in a running buffer consisting of 0.025 M Tris-HCl, 0.192 M glycine, and 0.1% SDS (pH 8.3). A constant current of 20 mA was applied during the stacking phase, followed by 30 mA during the resolving phase. Following electrophoresis, proteins were transferred onto polyvinylidene difluoride (PVDF) membranes through electrophoretic transfer for subsequent Western blot analysis.[48]

2.2.3.3. Protein transfer to PVDF membrane]

Following electrophoresis, the gel was incubated in transfer buffer composed of 39 mM glycine, 48 mM Tris base, 0.0375% SDS, and 20% methanol for 10 min to facilitate equilibration. Proteins were then transferred onto a PVDF membrane, pre-activated with methanol, and equilibrated in the same buffer. The transfer was performed using a semi-dry electroblotting system operated at a constant current of 0.8 mA/cm^2 for 1.5 h.

Transfer efficiency was verified by staining the membrane with Ponceau S solution containing 0.2% in 3% trichloroacetic acid and 3% sulfosalicylic acid. The positions of the molecular weight markers were marked on the blot before immunodetection.[48]

2.2.3.4. Western blot analysis and chemiluminescence detection

The membrane was extensively rinsed with 1× PBS to eliminate residual Ponceau S stain, followed by a blocking step in 5% Blotto solution – comprising 5% non-fat dry milk dissolved in Tris-buffered saline containing 0.1% Tween-20 (TBST) – for 1 h at room temperature to minimize non-specific antibody binding. Following blocking, the membrane was washed with TBST and incubated overnight at 4°C with the appropriate primary antibodies, including anti-Nrf2 antibody (1:1000 dilution), anti-FN3K antibody (1:1000 dilution), and anti-beta actin antibody (1:5000 dilution) as a loading control. After overnight incubation, the membranes were washed three times with TBST for 5 – 10 min each wash to remove unbound antibodies. Subsequently, the blots were incubated for 1 h at room temperature with horseradish peroxidase-conjugated goat anti-rabbit IgG secondary antibody, diluted 1:5000 in TBST. Following thorough washes with TBST to eliminate excess secondary antibody, protein bands were detected using a chemiluminescent substrate according to the manufacturer's protocol. Chemiluminescence signals were captured using a digital imaging system, and band intensities were analyzed for quantification. Beta actin served as a loading control for normalization of protein expression levels.[49]

2.3. Statistical analysis

All statistical evaluations were performed using Python libraries, including SciPy and statsmodels,[50] to assess the differential expression of FN3K and Nrf2 across various treatment groups in MCF-7, T-47D, BT-474, and Vero cell lines.

2.3.1. Data processing and normalization

In qPCR analysis, relative gene expression levels were calculated using the $2^{-}\Delta\Delta Ct$ method, with ACTB served as the internal control for normalization.[47] Meanwhile, for Western blot analysis, densitometric quantification of FN3K and Nrf2 protein bands was carried out using ImageJ (National Institutes of Health, Bethesda, USA). The values were normalized to beta actin to account for loading variability, and the resulting relative expression levels were subjected to statistical analysis.[50]

2.3.2. Statistical tests applied

Welch's t-test was employed to evaluate treatment effects by independently comparing each experimental group with the untreated control group. This statistical test

accommodates unequal variances and is appropriate for datasets with small sample sizes.[51] To mitigate the risk of false positives due to multiple comparisons, the Benjamini-Hochberg procedure was applied to control the False Discovery Rate (FDR).[52]

2.3.3. Significance thresholds used

The following significance thresholds were applied in the analysis: $p<0.05$ (*; marginally significant), $p<0.01$ (**; significant), $p<0.001$ (***; highly significant), $p\geq0.05$ → (not significant). All statistical analyses were conducted in Python utilizing the SciPy and statsmodels libraries, with statsmodels. stats. multitest applied for FDR correction.

3. Results and discussion

3.1. SBVS

3.1.1. Template selection and model validation

Template selection for homology modeling of the human FN3K enzyme was carried out by aligning the target protein sequence with evolutionarily related structures available in the SWISS-MODEL template library. To identify suitable homologous templates, the FN3K amino acid sequence was queried against the PDB-BLAST database. This search initially yielded 5,643 potential templates that matched the target sequence. To refine this extensive list, a heuristic approach was employed, narrowing it down to 50 templates. Figure 1 illustrates the alignment of the human FN3K target sequence with one of the selected homologous templates, highlighting the conserved regions and secondary structural elements.

Quality assessment of these 50 templates was performed using QMEAN and GMQE scores. QMEAN evaluates the overall geometric and energetic quality of the model, while GMQE estimates the expected accuracy of the homology model. Templates were ranked based on these criteria, with the top three templates demonstrating the highest scores and best alignment with the target sequence. In the subsequent protein modeling, three homology models (Figure 2) were developed, and the first model, based on the template from *Arabidopsis thaliana* FN3K, exhibited a sequence similarity of 90.61% with human FN3K and was selected for the study. This model was evaluated using GMQE and QMEAN scoring functions, where values approaching 1.0 on a scale from 0 to 1 indicate high model quality. The modeled protein structure (Model-1) achieved satisfactory scores, meeting the quality attributes necessary for a reliable model.

Further validation was carried out using the PROCHECK tool to assess the stereochemical quality of the model. PROCHECK provided a Ramachandran plot (Figure 3), which is instrumental in evaluating the overall geometry of the protein model based on residue-by-residue analysis of backbone dihedral angles (ϕ and ψ). The Ramachandran plot analysis revealed that most of the residues were located in the favored regions, indicating energetically favorable conformations. None of the residues were found in the disallowed or forbidden regions,

Figure 1. Target-template sequence alignment of human FN3K with a selected homologous structure (PDB ID: A0A2Y9PDG6.1.A). The figure displays the sequence alignment between the target human FN3K protein and its template, color-coded by region. Secondary structural elements (β-sheets) are shown as arrows. Conserved residues and aligned motifs critical for structural and functional integrity are evident across the alignment. This visualization supports the selection of a high-quality template for building the 3D model during the homology modeling process
Abbreviations: FN3K: Fructosamine-3-kinase

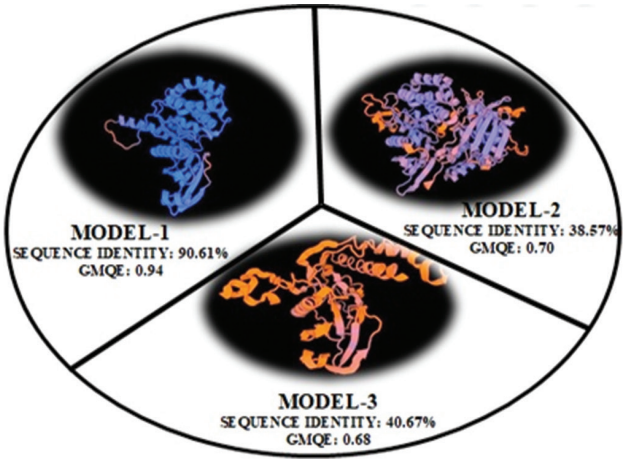

Figure 2. Comparative structural models of human FN3K derived from top-ranked homology templates. The figure illustrates three homology models generated during the structure prediction of human FN3K. Model-1 (top left): Based on a template from *Arabidopsis thaliana*, showing the highest sequence identity (90.61%) and a GMQE score of 0.94, indicating high structural reliability. Model-2 (top right): Built from a template with 38.57% sequence identity and a GMQE of 0.70. Model-3 (bottom): Constructed using a template with 40.67% identity and GMQE of 0.68
Abbreviations: FN3K: Fructosamine-3-kinase; GMQE: Global model quality estimation

confirming that the model meets the validation criteria for acceptable stereochemistry. Overall, the combination of high sequence similarity, favorable GMQE and QMEAN scores, and validation through PROCHECK suggests that Model-1 is a robust and accurate representation of the human FN3K enzyme structure. This structural model (Figure 4) provides a solid foundation for further computational and experimental studies aimed at understanding the functional implications and potential applications of human FN3K.

3.1.2. VS and docking results

SBVS yielded multiple candidate compounds with strong predicted binding affinities toward FN3K, as indicated by favorable docking scores. The selection criteria for potential hits included both numerical docking scores and qualitative assessments of key ligand–protein interactions, such as hydrogen bonding, hydrophobic contacts, and π–π stacking. Among the docked molecules, a subset exhibited significantly higher binding affinities and more favorable interaction profiles compared to others. To ensure the selection of the most potent inhibitors, a rank-based selection approach was applied, wherein the top 10% of ligands or the top 10 ranked compounds with the most negative Glide docking scores were shortlisted. This approach ensured that only the best-performing molecules – those predicted to have the highest binding affinity – were prioritized for

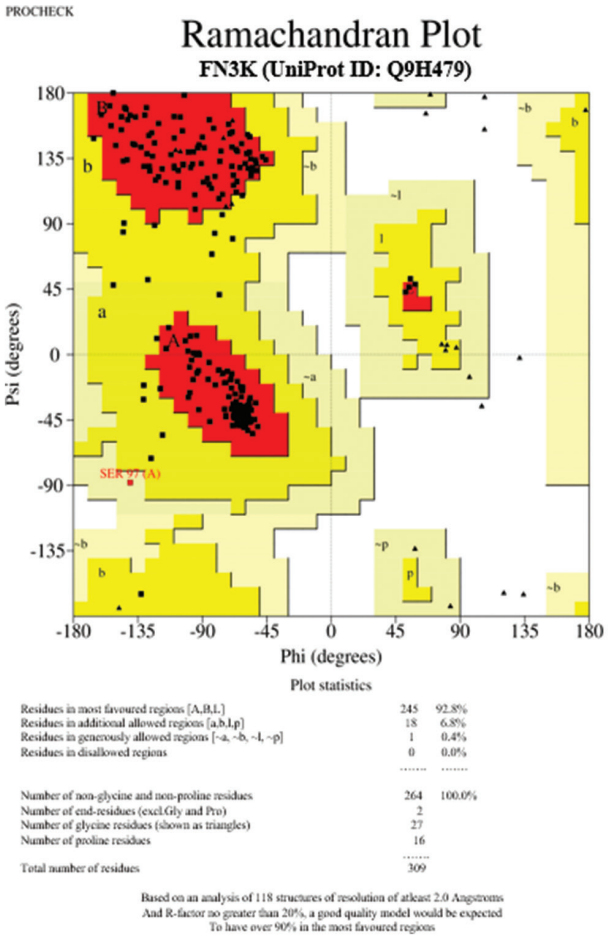

Figure 3. Ramachandran plot of the modeled human FN3K structure generated by PROCHECK. The plot depicts the distribution of backbone dihedral angles (ϕ and ψ) for amino acid residues in the modeled FN3K protein. Among 309 residues, 92.8% are located within the most favored regions, 6.8% within additionally allowed regions, and 0.4% within generously allowed regions. No residues were observed in disallowed regions, indicating the stereochemical validity of the predicted protein structure
Abbreviations: FN3K: Fructosamine-3-kinase

further evaluation. Table 2 summarizes the top six docked molecules, highlighting their docking scores, molecular weights, and specific amino acid interactions within the FN3K binding pocket. Notably, oxaliplatin, ritonavir, lansoprazole, and capivasertib demonstrated strong interactions with key residues, such as CYS A:24, LYS A:41, and ASP A:217 – suggesting a conserved binding motif critical for effective FN3K inhibition.

3.1.3. ADMET analysis of hit compounds

To further validate the potential hits, the top-ranked candidates were subjected to additional rounds of analysis. This included a review of their physicochemical properties

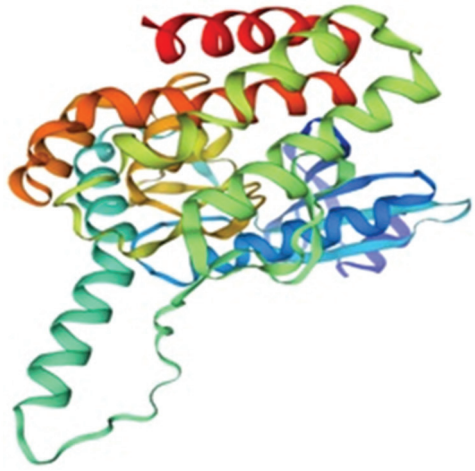

Figure 4. Three-dimensional structure of the final modeled human FN3K protein. The 3D structure is depicted using a rainbow color gradient, ranging from the N-terminus (blue) to the C-terminus (red), to illustrate the overall fold. The model features a compact globular conformation with prominent α-helices and β-sheets. Following validation by stereochemical and sequence-based assessments, this structure was chosen for subsequent molecular docking and functional analysis
Abbreviations: FN3K: Fructosamine-3-kinase

to ensure drug-likeness and a preliminary ADMET assessment to evaluate their pharmacokinetic profiles and safety considerations. The detailed results of the ADMET screening, including physicochemical properties, drug-likeness, solubility, gastrointestinal absorption, and cytochrome P450 (CYP) interactions, are provided in Supplementary Tables S1-S5 and Figure S1. These combined analyses enabled the exclusion of compounds with suboptimal properties or toxicity risks. Ultimately, the final selection of hit molecules was based on a holistic assessment encompassing VS performance, rank-based scoring, favorable physicochemical characteristics, and acceptable ADMET profiles. These molecules serve as promising leads for subsequent validation through *in vitro* enzyme inhibition assays and advanced computational analyses, aimed at substantiating their potential as therapeutic inhibitors of FN3K. Docking scores, expressed in kcal/mol, reflect the predicted binding affinity between ligand and target, with more negative values corresponding to stronger interactions.

3.1.4. Key findings from VS

Oxaliplatin (−9.2 kcal/mol) exhibited the highest binding affinity, forming stable interactions with residues CYS A:24, ILE A:25, LYS A:41, MET A:51, ASP A:217, and TRP A:219. These residues are likely critical for FN3K activity, suggesting a strong inhibitory potential. Lansoprazole (−8.6 kcal/mol) and capivasertib (−8.1 kcal/mol) also showed strong binding, interacting with CYS A:24, LYS A:41, and ASP A:217, which are key active site residues. This supports their potential as FN3K inhibitors. Ritonavir (−8.7 kcal/mol) demonstrated a strong binding score but interacted with fewer critical residues, indicating potential, but possibly with reduced specificity for FN3K inhibition. In contrast, amiloride (−6.9 kcal/mol) and 1-DMF (−6.1 kcal/mol) displayed weaker binding and fewer significant interactions, suggesting they may not be ideal candidates as FN3K inhibitor. The 3D and 2D protein–ligand interaction profiles of all six hit molecules, including their binding residues and docking scores, are presented in Figure S2.

This study was intentionally structured as a focused drug repurposing investigation aimed at identifying clinically relevant FN3K inhibitors with high translational potential. The screening FDA-approved kinase inhibitors, WHO-listed essential medicines, and anti-breast cancer agents offers multiple advantages in oncology drug discovery, including established safety profiles, known pharmacokinetic properties, and regulatory familiarity – factors that collectively expedite the clinical translation process. This strategic approach allowed us to rapidly transition from *in silico* screening to *in vitro* validation across diverse breast cancer subtypes.

Our findings with oxaliplatin, lansoprazole, and capivasertib underscore the feasibility and effectiveness of this repurposing-centric approach. These compounds demonstrated strong FN3K inhibition, selective cytotoxicity toward malignant cells, and downregulation of redox-associated transcriptional programs, thereby validating their mechanistic relevance.

Nonetheless, we acknowledge that restricting the chemical library to approved drugs inherently limits the structural diversity and novelty of potential hits. Exploring broader chemical space, including natural product scaffolds, macrocyclic inhibitors, and *de novo* designed chemical entities, may uncover novel binding chemotypes and allosteric inhibitors with improved specificity and potency. Accordingly, future studies will integrate VS of natural compound libraries (e.g., NPASS, ZINC Natural Products), fragment-based approaches, and machine learning-assisted scaffold hopping to identify next-generation FN3K inhibitors.

Thus, while our repurposing approach lays a pragmatic foundation for translational success, it also opens avenues for expanded pharmacophore discovery and rational design of structurally novel inhibitors tailored to FN3K's catalytic and regulatory domains.

Table 2. Docking scores and key interactions of selected hits with FN3K

S. No.	Drug name	Chemical structure	Docking score (kcal/mol)	Interacting amino acids
1	Oxaliplatin Mol wt: 397.2	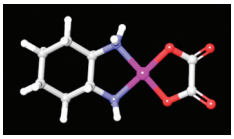	−9.2	CYS A: 24, ILE A: 25, LYS A: 41, MET A: 51, ASP A: 217, TRP A: 219
2	Ritonavir Mol wt: 720.31		−8.7	PHE A: 39, GLY A: 221
3	Lansoprazole Mol wt: 369.08	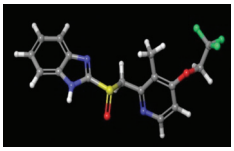	−8.6	CYS A: 24, LYS A: 41, ASP A: 217, TRP A: 219, HIS A: 288
4	Capivasertib Mol wt: 428.17	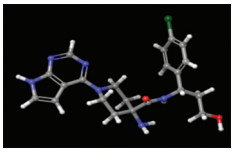	−8.1	CYS A: 24, LYS A: 41, ASP A: 217, GLY A: 221, ASN A: 222, ASP A: 234
5	Amiloride Mol wt: 229.05	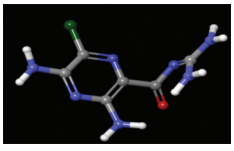	−6.9	CYS A: 24, ILE A: 25, SER A: 26, LYS A: 41, GLU A: 55, GLY A: 152, ASN A: 222
6	1-DMF Mol wt: 249.12	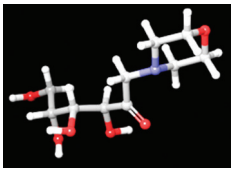	−6.1	GLY A: 221, ASP A: 234

Abbreviations: 1-DMF: 1-deoxy-morpholino-D-fructose; Mol wt: Molecular weight.

3.2. *In vitro* screening studies

3.2.1. Half-maximal inhibitory concentration (IC50) determination and cytotoxicity analysis

The cytotoxic effects of six selected compounds – 1-DMF, ritonavir, amiloride, lansoprazole, capivasertib, and oxaliplatin – were assessed across three breast cancer cell lines (MCF-7, T47D, and BT-474) and one non-malignant Vero cells using the MTT assay. IC_{50} values were calculated based on the percentage of viable cells relative to untreated controls. The IC_{50} values for each compound across the individual cell lines are summarized in Table 3.

All tested compounds exhibited concentration-dependent cytotoxicity across the evaluated breast cancer cell lines. Among them, oxaliplatin and lansoprazole demonstrated the lowest IC_{50} values (90 – 110 µg/mL), indicating a higher potency against MCF-7, T47D, and BT-474 cells. These results suggest that both compounds

Table 3. IC_{50} values (µg/mL) of selected compounds across different cell lines

Compounds	MCF-7	T47D	BT-474	Vero
1-DMF	125	125	125	>150
Ritonavir	125 – 150	125 – 150	125 – 150	>150
Amiloride	125 – 150	125 – 150	125 – 150	>150
Lansoprazole	90 – 110	90 – 110	90 – 110	150
Capivasertib	100 – 125	100 – 125	100 – 125	>150
Oxaliplatin	90 – 110	90 – 110	90 – 110	140

Abbreviations: 1-DMF: 1-deoxy-1-morpholino-D-fructose; IC_{50}: Half-maximal inhibitory concentration.

may be effective at lower concentrations in reducing cell viability and warrant further investigation as potential anti-cancer agents targeting FN3K pathways.

Capivasertib showed moderate cytotoxicity, with IC_{50} values ranging from 100 – 125 μg/mL across the tested breast cancer cell lines. On the other hand, ritonavir, amiloride, and 1-DMF exhibited higher IC_{50} values (125 – 150 μg/mL), suggesting relatively lower cytotoxic potential. Interestingly, the non-malignant Vero cells showed markedly higher IC_{50} values (>150 μg/mL for most compounds), indicating selective cytotoxicity toward cancer cells. This selective response enhances the potential therapeutic index of the effective compounds. Although the IC_{50} values observed for oxaliplatin and lansoprazole (~90 – 110 μg/mL) and for capivasertib (100 – 125 μg/mL), indicate promising *in vitro* potency, their pharmacological relevance must be interpreted with caution. Drug concentrations required to achieve cytotoxic effects in monolayer culture systems are often higher than those effective *in vivo*, due to differences in drug metabolism, microenvironmental factors, and tumor tissue architecture. Moreover, *in vitro* IC_{50} values do not account for sustained exposure, tissue retention, or intracellular accumulation – all of which significantly influence therapeutic outcomes in clinical settings.

For instance, oxaliplatin forms DNA adducts that persist long after plasma clearance, contributing to prolonged anti-tumor activity.[53] Capivasertib has demonstrated efficacy in breast cancer clinical trials with intermittent oral dosing (400 – 480 mg BID), showing favorable toxicity profiles.[54] Lansoprazole, although not classified as an anti-cancer drug, has exhibited synergistic effects with chemotherapeutics in pre-clinical models due to its modulation of lysosomal pH and autophagy.[55]

Therefore, while the IC_{50} values provide a useful benchmark for early-stage screening, *in vivo* pharmacokinetic and tumor accumulation studies are essential for confirming therapeutic relevance. Our future animal studies will evaluate FN3K–Nrf2 axis modulation, assess systemic toxicity, and establish optimal dosing strategies to bridge the current gap between *in vitro* and *in vivo* findings.

To further assess treatment-induced effects, microscopic images of both treated and untreated cells were captured. These images, provided in Supplementary Figures S3 and S4, depict the cellular morphological changes observed post-treatment. However, as this study primarily focuses on the molecular downregulation of FN3K expression, further analyses were conducted using qPCR and Western blot techniques.

3.2.2. qPCR analysis

3.2.2.1. FN3K and Nrf2 expression in MCF-7 Cells

qPCR was conducted to assess the modulatory effects of six tested compounds on the gene expression levels of FN3K and Nrf2 in MCF-7 breast cancer cells. The integrity of the isolated RNA was validated through agarose gel electrophoresis (Supplementary Figure S5).

The expression patterns of FN3K and Nrf2 were evaluated across different treatment conditions, revealing distinct regulatory effects. In the untreated control, FN3K and Nrf2 exhibited baseline expression levels of 1.000 and 1.020, respectively. Among the tested compounds, oxaliplatin, lansoprazole, and capivasertib emerged as potent FN3K inhibitors. Oxaliplatin exhibited the most significant suppression, reducing FN3K expression by nearly 99.99% (2.0×10^{-5}), along with a moderate Nrf2 suppression (0.032). Similarly, lansoprazole showed strong FN3K inhibition, with a 99.90% reduction (0.001), accompanied by a mild decrease in Nrf2 expression (0.015). Capivasertib also demonstrated substantial FN3K suppression (0.000), along with moderate Nrf2 inhibition (0.063), making its efficacy comparable to that of the other top inhibitors. These findings confirm that oxaliplatin, lansoprazole, and capivasertib act as effective FN3K inhibitors, capable of significantly reducing FN3K expression with varying degrees of Nrf2 suppression. This is illustrated in Supplementary Figure S6, which presents qPCR gel images of FN3K and Nrf2 expression.

Conversely, amiloride, ritonavir, and 1-DMF did not exhibit strong FN3K inhibition, with some compounds showing unexpected regulatory effects. Amiloride led to a 157.0% increase in FN3K expression (2.570), while simultaneously inducing marked suppression of Nrf2 (7.4×10^{-5}), suggesting a potential inverse regulatory mechanism. Similarly, ritonavir induced a slight upregulation of FN3K (1.220), along mild Nrf2 suppression (0.001), indicating no inhibitory effect on FN3K. Meanwhile, 1-DMF displayed moderate FN3K suppression (0.176), but only weak inhibition of Nrf2 (0.022), making it less potent compared to oxaliplatin, lansoprazole, and capivasertib.

Since FN3K inhibition was the primary objective of this study, only compounds demonstrating significant FN3K downregulation in MCF-7 cells were selected for further qPCR analysis. Among the six tested compounds, oxaliplatin, lansoprazole, and capivasertib exhibited potent FN3K suppression (≥99.6%), whereas amiloride and ritonavir failed to inhibit FN3K, and 1-DMF showed only moderate inhibition.

To substantiate these observations and examine the consistency of FN3K inhibition across distinct breast

cancer subtypes, qPCR analysis was further performed on T-47D and BT-474 cell lines. Vero cells were incorporated as a non-malignant control model to evaluate the selectivity of the tested compounds toward malignant cells.

3.2.2.2. FN3K and Nrf2 expression in T-47D Cells

The impact of oxaliplatin, lansoprazole, and capivasertib on the expression of FN3K and Nrf2 was assessed in T-47D cells, demonstrating a consistent downregulation of FN3K, comparable to the pattern observed in MCF-7 cells. In the untreated control group, baseline expression levels were recorded as 1.010 for FN3K and 1.060 for Nrf2. Among the tested compounds, lansoprazole displayed the highest degree of FN3K inhibition, reducing expression by 99.99% (1.00×10^{-4}), along with significant suppression of Nrf2 (0.029, ↓97.2%). Oxaliplatin also exhibited potent FN3K downregulation (↓99.6%), reducing FN3K expression to 0.004, with corresponding Nrf2 suppression of 0.028 (↓97.3%). Similarly, capivasertib strongly inhibited FN3K expression (↓99.97%), reducing it to 2.60×10^{-4}, with a moderate suppression of Nrf2 (0.056, ↓94.7%).

These results indicate that FN3K suppression by lansoprazole, oxaliplatin, and capivasertib in T-47D cells is consistent with trends observed in MCF-7 cells. Notably, lansoprazole demonstrated the highest FN3K inhibition in T-47D (↓99.99%), exceeding its effect in MCF-7 cells, further reinforcing its potential as a potent FN3K inhibitor. Similarly, oxaliplatin and capivasertib maintained strong FN3K suppression across both cell lines (↓99.6 – 99.99%), confirming their effectiveness in targeting FN3K-dependent pathways. These findings suggest that FN3K inhibition by these compounds is not restricted to a specific cell line but represents a consistent biological response, further validating their therapeutic relevance.

3.2.2.3. FN3K and Nrf2 expression in BT-474 Cells

The expression patterns of FN3K and Nrf2 were analyzed in BT-474 cells following treatment with oxaliplatin, lansoprazole, and capivasertib, revealing strong and consistent downregulation of FN3K across all tested conditions. In the untreated control group, baseline expression levels of FN3K and Nrf2 were 1.020 and 1.050, respectively. Lansoprazole demonstrated the most potent FN3K inhibition, reducing its expression by 99.98% to 0.000, while also significantly suppressing Nrf2 to 0.060, representing a 94.3% reduction. Oxaliplatin also showed strong FN3K suppression, reducing expression by 99.7% to 0.003, with Nrf2 downregulated to 0.104, corresponding to a 90.1% decrease. Similarly, capivasertib exhibited substantial FN3K inhibition of 99.88%, lowering expression to 0.001, and moderately suppressing Nrf2 to 0.067, representing a 93.5% reduction.

These findings further reinforce the consistency of FN3K inhibition across multiple breast cancer cell lines. Lansoprazole consistently exhibited the highest FN3K suppression across MCF-7, T-47D, and BT-474 models, with inhibition levels ranging from 99.98% to 99.99%. Similarly, oxaliplatin and capivasertib maintained robust and reproducible FN3K inhibition across all cell lines, with suppression levels ranging from 99.6% to 99.99%. The consistency of these results across various breast cancer subtypes – including ER-positive, HER2-positive, and triple-negative models – indicates the broad-spectrum potential of these compounds as FN3K inhibitors, thereby reinforcing their prospective therapeutic value in various breast cancer settings.

3.2.2.4. FN3K and Nrf2 expression in Vero cells

The expression patterns of FN3K and Nrf2 in Vero cells were assessed following treatment with oxaliplatin, lansoprazole, and capivasertib. In contrast to the strong inhibitory effects observed in breast cancer cell lines, these compounds exhibited minimal to no suppression of FN3K in Vero cells. In the untreated control group, baseline expression levels of FN3K and Nrf2 were 1.040 and 1.000, respectively. Oxaliplatin resulted in a modest 12% reduction in FN3K expression, lowering it to 0.880, while Nrf2 remained unchanged at 1.010, indicating no significant impact on this pathway. Lansoprazole caused a slight FN3K suppression of 9%, reducing expression to 0.910, and also mildly inhibited Nrf2 to 0.890, representing an 11% decrease. Capivasertib did not alter FN3K expression, which remained at 1.010, and induced only a minor suppression in Nrf2 to 0.950, representing a 5% decrease.

These results suggest that FN3K inhibition by oxaliplatin, lansoprazole, and capivasertib is not prominent in non-malignant Vero cells, in stark contrast to their effects in breast cancer models. The lack of substantial FN3K suppression in Vero cells indicates a degree of specificity toward malignant cells, as observed in MCF-7, T-47D, and BT-474. Furthermore, the minimal changes in Nrf2 expression across treatments further support the idea that these compounds may exert selective effects depending on the cellular context. These observations underscore the differential regulatory effects of the tested compounds on FN3K and Nrf2 expression in cancerous versus non-cancerous cell lines, supporting their therapeutic potential in cancer management while indicating a comparatively minimal impact on normal cells.

3.2.3. Comparative analysis of FN3K and Nrf2 downregulation: Cancer vs. normal cells

qPCR was employed to investigate the expression patterns of FN3K and Nrf2 in three human breast cancer cell lines

– MCF-7, T-47D, and BT-474 – as well as in the non-malignant Vero cell line. This analysis aimed to explore the differential modulation of FN3K and Nrf2 following treatment with oxaliplatin, lansoprazole, and capivasertib, thereby evaluating both the selectivity and efficacy of these agents in targeting cancerous versus non-cancerous cells.

As shown in Table 4, all three compounds significantly suppressed FN3K and Nrf2 expression in the breast cancer cell lines, with lansoprazole and oxaliplatin showing the most potent effects. Notably, the FN3K fold changes in cancer cells decreased by more than 99% across all three treatments, while expression in Vero cells remained largely unaffected, highlighting their selective activity toward malignant cells. Similar trends were observed for Nrf2, with up to 98.5% downregulation in cancer lines and only minimal suppression observed in the Vero cell line.

This comparative analysis provides critical insights into the therapeutic potential of FN3K-targeted inhibition and its downstream impact on Nrf2-regulated oxidative stress pathways, which are often upregulated in cancer cells to promote survival and resistance to therapy.

3.2.3.1. FN3K inhibition exhibits high selectivity for cancer cells with minimal effects in normal cells

As shown in Table 4, oxaliplatin, lansoprazole, and capivasertib all demonstrated strong FN3K downregulation (↓99.6 – 99.99%) in breast cancer cell lines. In contrast, FN3K expression in non-malignant Vero cells remained largely unaffected, with only a modest reduction of 9 – 12%. These findings indicate that FN3K inhibition by these compounds exhibits tumor-selective activity, potentially minimizing the risk of off-target effects in non-cancerous cells.

3.2.3.2. Nrf2 inhibition follows FN3K suppression selectively in cancer cells

In cancer cells, Nrf2 expression was significantly downregulated (↓90.1 – 98.5%) following treatment with the tested compounds. In Vero cells, however, Nrf2 expression level remained unchanged or was only mildly suppressed (↓5 – 11%). This pattern further supports the selectivity of FN3K-targeting compounds for tumor suppression.

3.2.3.3. Capivasertib demonstrates the highest FN3K selectivity among the tested compounds

Among the three compounds, capivasertib exhibited the greatest selectivity. In breast cancer cells (MCF-7, T-47D, BT-474), capivasertib strongly inhibited FN3K expression (↓99.88 – 99.98%). In contrast, FN3K expression in Vero cells remained unchanged, indicating no significant impact on non-malignant cells. This suggests that capivasertib may serve as the most specific FN3K inhibitor among the three.

3.3. Statistical analysis

3.3.1. Differential expression of FN3K and Nrf2 in MCF-7 Cells

qPCR analysis of FN3K and Nrf2 gene expression in MCF-7 breast cancer cells treated with oxaliplatin, lansoprazole, capivasertib, amiloride, ritonavir, and 1-DMF demonstrated notable alterations in transcript levels. Statistical evaluation was performed using either Welch's

Table 4. Comparative qPCR analysis of FN3K and Nrf2 downregulation in cancer (MCF-7, T-47D, BT-474) versus normal (Vero) cells

Treatment	FN3K fold change (MCF-7)	FN3K fold change (T-47D)	FN3K fold change (BT-474)	FN3K fold change (Vero)	Interpretation
Untreated (control)	1.00	1.01	1.02	1.04	Baseline expression in all cell lines.
Oxaliplatin	0.00002 (↓99.99%)	0.0039 (↓99.6%)	0.0029 (↓99.7%)	0.88 (↓12%)	Selective FN3K inhibition in cancer cells, minimal effect in Vero cells.
Lansoprazole	0.00097 (↓99.90%)	0.0001 (↓99.99%)	0.0002 (↓99.98%)	0.91 (↓9%)	Highly selective FN3K inhibition in cancer cells, minimal suppression in Vero cells.
Capivasertib	0.00017 (↓99.98%)	0.00026 (↓99.97%)	0.0012 (↓99.88%)	1.01 (No change)	Strong FN3K suppression in cancer cells, no effect in Vero cells.
Treatment	Nrf2 fold change (MCF-7)	Nrf2 fold change (T-47D)	Nrf2 fold change (BT-474)	Nrf2 fold change (Vero)	Interpretation
Untreated (Control)	1.02	1.06	1.05	1.00	Baseline expression in all cell lines.
Oxaliplatin	0.0318 (↓96.8%)	0.0283 (↓97.3%)	0.1041 (↓90.1%)	1.01 (No change)	Selective Nrf2 inhibition in cancer cells, no effect in Vero cells.
Lansoprazole	0.0152 (↓98.5%)	0.0289 (↓97.2%)	0.0595 (↓94.3%)	0.89 (↓11%)	Strong Nrf2 inhibition in cancer cells, mild effect in Vero cells.
Capivasertib	0.0629 (↓93.8%)	0.0563 (↓94.7%)	0.0673 (↓93.5%)	0.95 (↓5%)	Significant Nrf2 suppression in cancer cells, minimal effect in Vero cells.

Note: ↓indicates percent downregulation in gene expression relative to control (untreated) levels.
Abbreviation: FN3K: Fructosamine-3-kinase.

t-test or the Mann-Whitney U test, with adjustments for multiple comparisons made through FDR correction.

3.3.1.1. FN3K expression analysis

The expression of FN3K was significantly downregulated upon treatment with oxaliplatin, lansoprazole, and capivasertib, with all three compounds showing highly significant reductions (p<0.001; Figure 5). In contrast, 1-DMF exhibited a marginally significant reduction in FN3K expression (p<0.05). Neither amiloride (p=0.092) nor ritonavir (p=0.199) significantly altered FN3K expression following FDR correction. These findings suggest that oxaliplatin, lansoprazole, and capivasertib act as effective FN3K inhibitors, whereas amiloride and ritonavir do not substantially influence FN3K levels in MCF-7 cells.

3.3.1.2. Nrf2 expression analysis

The expression of Nrf2 was significantly downregulated by lansoprazole, amiloride, and ritonavir, with all three compounds demonstrating highly significant reductions (p<0.001; Figure 5). Oxaliplatin also suppressed Nrf2 expression but to a lesser extent, with statistical significance at p<0.01. Meanwhile, 1-DMF exhibited a marginally significant reduction (p<0.05). Capivasertib, however, did not significantly alter Nrf2 expression (p=0.171). Interestingly, although amiloride and ritonavir did not significantly impact FN3K expression, both compounds caused a pronounced suppression of Nrf2, suggesting a potential alternative regulatory mechanism.

These results highlight that oxaliplatin, lansoprazole, and capivasertib effectively inhibit FN3K, while lansoprazole, amiloride, and ritonavir strongly suppress Nrf2. The differential effects observed indicate that while some compounds act directly on FN3K, others may influence Nrf2 independently, warranting further mechanistic exploration.

3.3.2. Differential expression of FN3K and Nrf2 in T-47D Cells

3.3.2.1. FN3K expression analysis

The expression of FN3K was significantly downregulated by oxaliplatin, lansoprazole, and capivasertib, with all three treatments displaying highly significant reductions (p<0.001; Figure 6). This strong statistical significance indicates that these compounds may act as potent FN3K inhibitors in T-47D cells, reinforcing their inhibitory effects observed in other breast cancer cell models.

3.3.2.2. Nrf2 expression analysis

Oxaliplatin, lansoprazole, and capivasertib all significantly downregulated Nrf2 expression, with p-values falling below the 0.01 threshold after FDR correction (Figure 6).

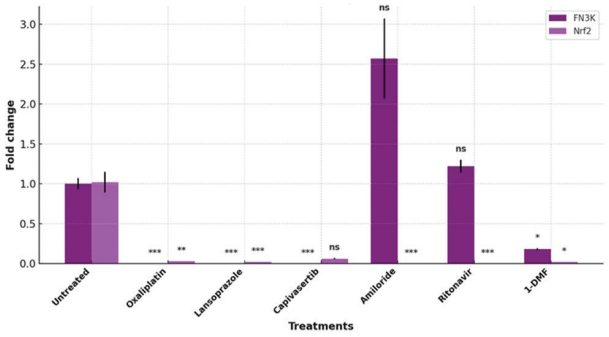

Figure 5. Treatment-specific expression of *FN3K* and *Nrf2* genes in MCF-7 cells. The bar graph illustrates the fold change in FN3K and Nrf2 expression following treatment with oxaliplatin, lansoprazole, capivasertib, amiloride, ritonavir, and 1-DMF. Significant downregulation of FN3K was observed with oxaliplatin, lansoprazole, and capivasertib (p<0.001), while Nrf2 expression was significantly reduced by lansoprazole, amiloride, and ritonavir (p<0.001)
Abbreviations: 1-DMF: 1-deoxy-1-morpholino-D-fructose; FN3K: Fructosamine-3-kinase; Nrf2: Nuclear factor erythroid 2-related factor 2; ns: Not significant

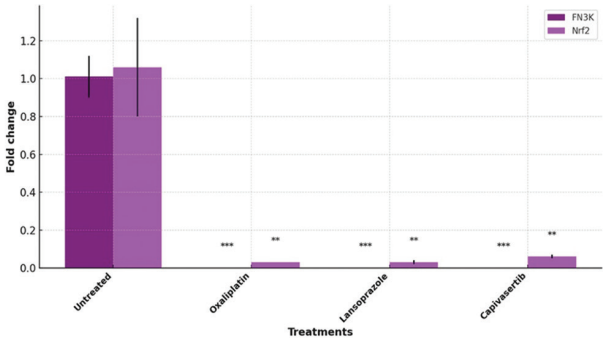

Figure 6. Treatment-specific expression of *FN3K* and *Nrf2* genes in T-47D cells. FN3K and Nrf2 expression were significantly reduced in response to oxaliplatin, lansoprazole, and capivasertib (p<0.001 for FN3K; p<0.01 for Nrf2), suggesting a strong inhibitory effect
Abbreviations: FN3K: Fructosamine-3-kinase; Nrf2: Nuclear factor erythroid 2-related factor 2

This consistent suppression of Nrf2 suggests that these compounds may exert a dual effect by not only inhibiting FN3K but also reducing Nrf2 levels in T-47D cells. The concurrent inhibition of both FN3K and Nrf2 may enhance the therapeutic relevance of these compounds by targeting key regulatory pathways involved in cancer progression.

3.3.3. Differential expression of FN3K and Nrf2 in BT-474 Cells

3.3.3.1. FN3K expression analysis

The expression of FN3K was significantly downregulated by oxaliplatin, lansoprazole, and capivasertib, with all three treatments displaying highly significant reductions

(p<0.001; Figure 7). The strong statistical significance across these treatments suggests that these compounds act as potent FN3K inhibitors in BT-474 cells, consistent with findings in other breast cancer models. This reinforces their potential as effective FN3K-targeting agents.

3.3.3.2. Nrf2 expression analysis

Oxaliplatin, lansoprazole, and capivasertib all significantly downregulated Nrf2 expression, with p-values falling below 0.01 after FDR correction (Figure 7). This suggests that these compounds not only inhibit FN3K but also reduce Nrf2 levels in BT-474 cells. The simultaneous suppression of FN3K and Nrf2 may enhance their therapeutic potential by targeting key pathways involved in tumor progression, further supporting their role as promising candidates for cancer therapy.

3.3.4. Differential expression of FN3K and Nrf2 in Vero Cells

3.3.4.1. FN3K expression analysis

FN3K expression did not show significant downregulation in response to oxaliplatin, lansoprazole, or capivasertib, as all treatments resulted in p-values greater than 0.05, indicating no statistical significance (Figure 8). This suggests that these compounds do not significantly affect FN3K expression in Vero cells, a non-malignant model. The absence of FN3K suppression in normal cells further supports the hypothesis that the inhibitory effects observed in breast cancer models may be tumor-specific.

3.3.4.2. Nrf2 expression analysis

Similarly, no significant downregulation of Nrf2 expression was observed in response to oxaliplatin, lansoprazole, or capivasertib, with all p-values exceeding 0.05 (Figure 8). This indicates that these compounds do not exhibit inhibitory effects on Nrf2 expression in Vero cells. Given that Vero cells are non-malignant, these findings reinforce the idea that FN3K and Nrf2 inhibition observed in breast cancer models may be selective for cancerous cells, further strengthening their potential relevance in oncological applications.

3.4. Western blot

Western blot analysis was conducted to quantify FN3K and Nrf2 protein expression levels in MCF-7, BT-474, and T-47D breast cancer cell lines, as well as in Vero cells to assess specificity. The initial analysis was performed in MCF-7 cells to evaluate the expression levels of FN3K and Nrf2 following treatment with six hit molecules identified from the *in silico* VS. Based on the expression patterns observed, a subset of these compounds was chosen for

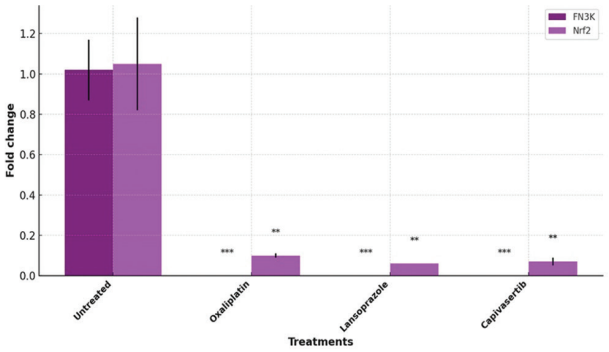

Figure 7. Treatment-specific expression of *FN3K* and *Nrf2* genes in BT-474 cells. The expression levels of FN3K and Nrf2 were significantly downregulated following treatment with oxaliplatin, lansoprazole, and capivasertib (p<0.001 for FN3K; p<0.01 for Nrf2)
Abbreviations: FN3K: Fructosamine-3-kinase; Nrf2: Nuclear factor erythroid 2-related factor 2

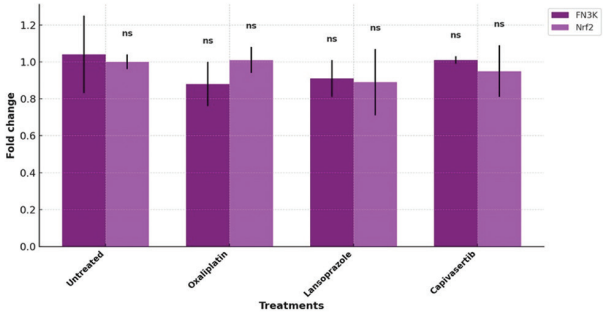

Figure 8. Treatment-specific expression of FN3K and Nrf2 in Vero cells. The bar graph represents the fold change in expression levels upon treatment with oxaliplatin, lansoprazole, and capivasertib. No statistically significant changes were observed across treatments
Abbreviations: FN3K: Fructosamine-3-kinase; Nrf2: Nuclear factor erythroid 2-related factor 2; ns: Not significant

further validation in BT-474 and T-47D breast cancer cell lines to assess the consistency of their effects across different breast cancer models. In addition, the selected compounds were tested in Vero cells to evaluate their specificity and ensure that the observed effects were cancer cell-specific rather than a generalized cellular effect.

3.4.1. Western blot analysis of FN3K and Nrf2 expression in MCF-7 Cells

Western blot analysis revealed distinct expression patterns of FN3K and Nrf2 across different treatment groups, highlighting potential mechanisms of action for the tested compounds. The primary FN3K inhibitors demonstrated substantial downregulation of FN3K (Figure 9), whereas the impact on Nrf2 varied among treatments (Figure 10), indicating distinct regulatory influences on metabolic and oxidative stress pathways.

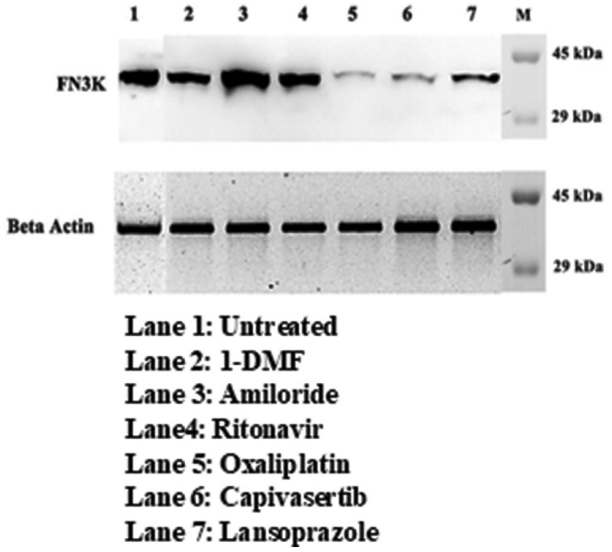

Figure 9. Representative Western blot showing FN3K protein expression following treatment with various compounds. Cell lysates were subjected to SDS-PAGE and probed with anti-FN3K antibody. Beta actin was used as a loading control. A molecular weight marker (lane M) is included for size reference (29 kDa and 45 kDa)
Abbreviations: 1-DMF: 1-deoxy-1-morpholino-D-fructose; FN3K: Fructosamine-3-kinase

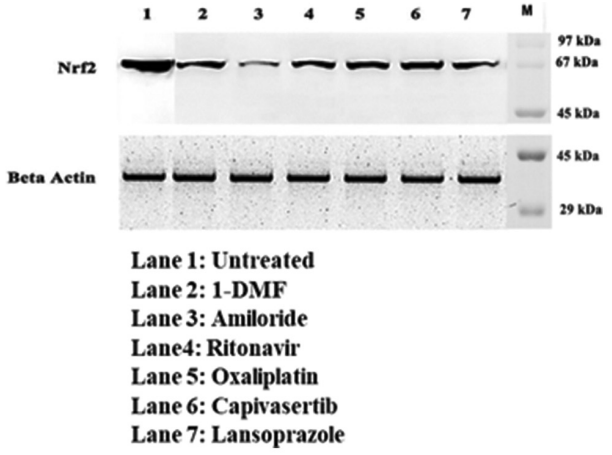

Figure 10. Representative Western blot showing Nrf2 protein expression under different treatment conditions. Cell lysates were analyzed by SDS-PAGE and immunoblotted with an anti-Nrf2 antibody. Beta actin was used as a loading control. A molecular weight marker (lane M) was included for reference, indicating band positions at 29, 45, 67, and 97 kDa
Abbreviations: 1-DMF: 1-deoxy-1-morpholino-D-fructose; Nrf2: Nuclear factor erythroid 2-related factor 2

3.4.1.1. FN3K expression analysis

FN3K expression was markedly reduced by oxaliplatin (0.322), capivasertib (0.317), and lansoprazole (0.457), indicating a strong inhibitory effect (Figure 9). Among these, oxaliplatin exhibited the most potent suppression, reducing FN3K levels by approximately 66% relative to the untreated control, closely followed by capivasertib. These findings suggest that FN3K inhibition may be a key mechanism underlying the anti-cancer activity of oxaliplatin and capivasertib. Moderate suppression of FN3K expression was observed with 1-DMF (0.636) and ritonavir (0.834), indicating a less pronounced but still notable inhibitory effect. This suggests that while these compounds interfere with FN3K function, their effects are weaker compared to oxaliplatin and capivasertib. In contrast, amiloride (0.976) had minimal impact on FN3K expression, implying that its mechanism of action does not involve FN3K inhibition and may instead act through alternative metabolic or signaling pathways.

3.4.1.2. Nrf2 expression analysis

Nrf2 expression exhibited the most significant reduction following treatment with amiloride (0.393), representing nearly a 60% decrease relative to the untreated control (Figure 10). This drastic downregulation suggests that amiloride may interfere with oxidative stress-related pathways, potentially sensitizing MCF-7 cells to oxidative stress and impairing adaptive responses that promote chemoresistance.

Moderate reductions in Nrf2 expression were observed with 1-DMF (0.639), ritonavir (0.584), and lansoprazole (0.683). The suppression induced by lansoprazole (~30% reduction) aligns with previous studies suggesting that proton pump inhibitors can modulate oxidative stress and apoptosis-related mechanisms. In contrast, oxaliplatin (0.818) and capivasertib (0.812) did not significantly suppress Nrf2 expression, with levels remaining close to those of the untreated control. This suggests that while these compounds effectively inhibit FN3K, they do not substantially impair oxidative stress defenses, indicating a more selective mechanism of action. The observed variations in FN3K and Nrf2 expression across different treatment conditions provide valuable insights into the mechanistic pathways influenced by these compounds. The differential effects on FN3K and Nrf2 suggest potential therapeutic implications, with some compounds acting primarily as FN3K inhibitors, while others modulating oxidative stress responses, both of which may contribute to their overall anti-cancer potential.

3.4.2. Western blot analysis of FN3K and Nrf2 expression in T-47D Cells

Western blot analysis was carried out to quantify FN3K and Nrf2 protein expression in T-47D cells following treatment with the selected compounds. The result revealed distinct expression patterns of FN3K and Nrf2 across the different

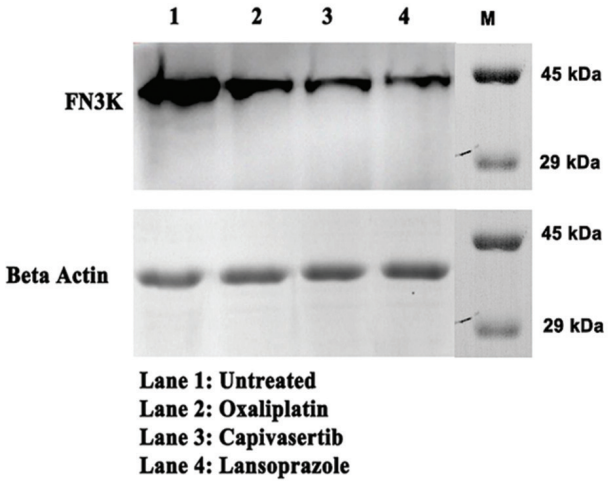

Figure 11. Representative Western blot showing FN3K protein levels in T47D cells treated with different compounds. T47D cell lysates were subjected to SDS-PAGE and immunoblotted using an anti-FN3K antibody. Beta actin was used as a loading control. A molecular weight marker (lane M) is included for size reference (29 kDa and 45 kDa)
Abbreviations: FN3K: Fructosamine-3-kinase

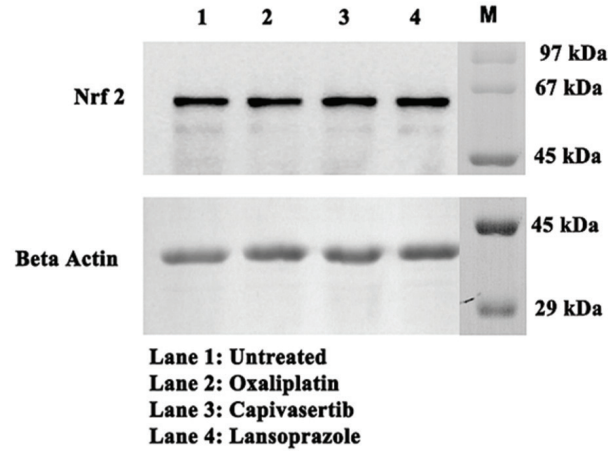

Figure 12. Representative Western blot showing Nrf2 protein expression in T47D cells treated with selected compounds. Western blot analysis was performed using T47D cell lysates probed with an anti-Nrf2 antibody. Beta actin was used as the internal loading control. A molecular weight marker (M) indicates bands at 29, 45, 67, and 97 kDa
Abbreviations: Nrf2: Nuclear factor erythroid 2-related factor 2

treatment groups, highlighting potential mechanisms of action for the tested compounds, as depicted in Figures 11 and 12.

3.4.2.1. FN3K expression analysis

Oxaliplatin exhibited the most substantial reduction in FN3K expression, decreasing its levels to 0.677, which representing approximately a 30% suppression compared to the untreated control (Figure 11). This suggests that oxaliplatin may act as a strong FN3K inhibitor in T-47D cells, potentially influencing metabolic regulation. In contrast, capivasertib (0.979) and lansoprazole (0.876) induced only minimal reductions in FN3K expression, with lansoprazole showing a modest ~10% decrease, while capivasertib had a negligible effect. These findings indicate that while these compounds may modulate FN3K expression, their impact is less pronounced than that observed with oxaliplatin. The untreated control (0.967) served as a baseline reference for comparison.

3.4.2.2. Nrf2 expression analysis

Nrf2 expression remained largely unaffected across all treatment groups, with oxaliplatin (0.909), capivasertib (0.979), and lansoprazole (0.886) showing values close to or slightly below control levels (1.049; Figure 12). This suggests that, in T-47D cells, these compounds do not significantly influence Nrf2 expression, contrasting with their observed effects in other cell models.

A notable difference was observed when comparing these findings to MCF-7 cells, where amiloride significantly suppressed Nrf2 expression (~60% reduction), and both oxaliplatin and capivasertib induced moderate reductions (~20%). In T-47D cells, however, none of the tested compounds produced significant Nrf2 downregulation, indicating potential cell-line-specific resistance mechanisms or a lack of regulatory dependency between FN3K suppression and Nrf2 modulation in this model. These findings highlight differences in FN3K and Nrf2 regulatory pathways between MCF-7 and T-47D cells, suggesting that cell-line-specific responses should be considered when evaluating FN3K inhibitors for therapeutic applications.

3.4.3. Western blot analysis of FN3K and Nrf2 expression in BT-474 Cells

Western blot analysis was conducted to evaluate FN3K and Nrf2 expression levels in BT-474 cells under different treatment conditions. The results (Figures 13 and 14) illustrate distinct regulatory effects, with FN3K expression exhibiting variable suppression across treatments, while Nrf2 levels remained largely stable.

3.4.3.1. FN3K expression analysis

Oxaliplatin exhibited the most pronounced suppression of FN3K expression, reducing its levels to 0.681, corresponding to an approximately 30% reduction compared to the untreated control (Figure 13). This suggests that oxaliplatin effectively inhibits FN3K,

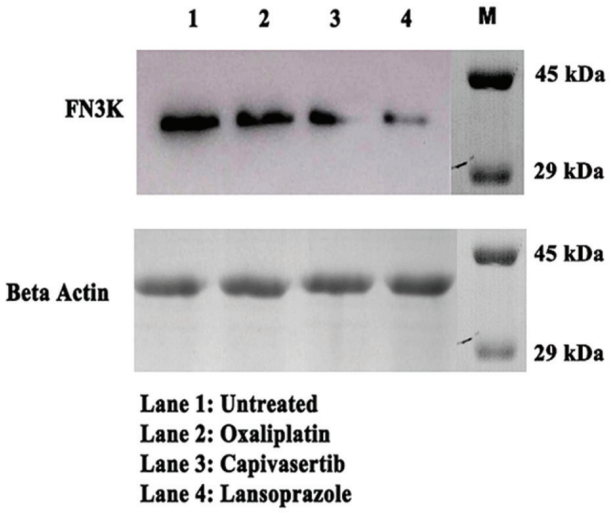

Figure 13. Representative Western blot showing FN3K expression in BT474 cells treated with different compounds. Protein lysates from BT474 cells were separated by SDS-PAGE and immunoblotted with an anti-FN3K antibody. Beta actin served as the internal loading control. A molecular weight marker (lane M) is included for size reference (29 kDa and 45 kDa)
Abbreviations: FN3K: Fructosamine-3-kinase

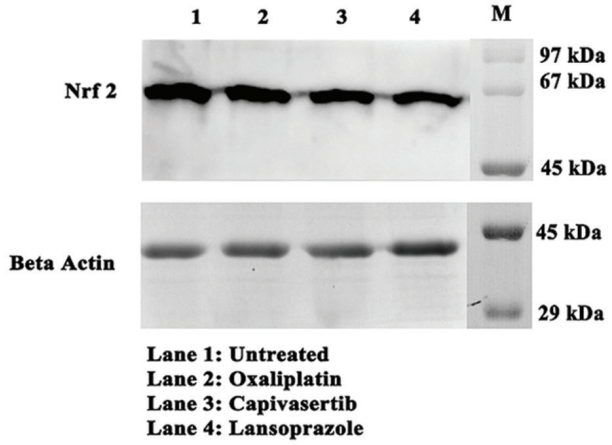

Figure 14. Representative Western blot showing Nrf2 protein expression in BT474 cells after compound treatment. BT474 cell lysates were analyzed by SDS-PAGE and probed with an anti-Nrf2 antibody. Beta actin was used as a loading control. A molecular weight marker (M) indicates bands at 29, 45, 67, and 97 kDa
Abbreviations: Nrf2: Nuclear factor erythroid 2-related factor 2

potentially disrupting metabolic adaptation mechanisms in BT-474 cells. Lansoprazole (0.802) induced a moderate reduction (~17% decrease), indicating some level of inhibition, though less pronounced than oxaliplatin. In contrast, capivasertib (0.991) resulted in a negligible reduction (~2% decrease), suggesting that it does not significantly affect FN3K levels in BT-474 cells.

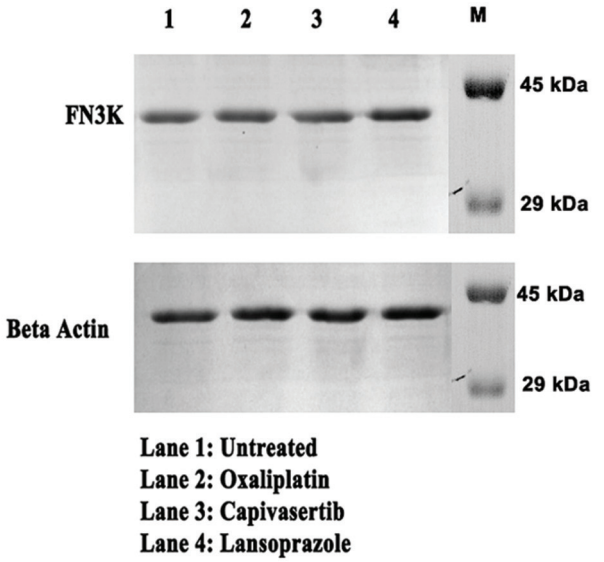

Figure 15. Representative Western blot showing FN3K expression in Vero cells after treatment with selected compounds. Vero cell lysates were subjected to SDS-PAGE and immunoblotting using an anti-FN3K antibody. Beta actin served as a loading control. A molecular weight marker (lane M) is included for size reference (29 kDa and 45 kDa)
Abbreviations: FN3K: Fructosamine-3-kinase

3.4.3.2. Nrf2 expression analysis

Nrf2 expression remained largely unchanged across all treatment groups, with oxaliplatin (0.917), capivasertib (1.008), and lansoprazole (0.964) displaying values close to those of the untreated control (1.049; Figure 14). This indicates that these compounds do not significantly downregulate Nrf2 in BT-474 cells. The stability of Nrf2 levels suggests the presence of a resistance mechanism in this cell line that prevents oxidative stress suppression, distinguishing BT-474 from other models.

These findings underscore the distinct regulatory responses in BT-474 cells compared to MCF-7 and T-47D, emphasizing the importance of considering cell-line-specific variations in FN3K and Nrf2 modulation when evaluating therapeutic strategies.

3.4.4. Western blot analysis in Vero cells: Assessing specificity and off-target effects

Vero cells, derived from the kidney epithelium of the African green monkey, serve as a non-malignant control model in comparative studies. Unlike cancer cells, Vero cells exhibit distinct metabolic and oxidative stress response mechanisms, allowing them suitable for assessing potential off-target effects and the cancer selectivity of tested compounds. Evaluating FN3K and Nrf2 modulation in Vero cells following treatment with oxaliplatin, capivasertib, and lansoprazole provides valuable insights

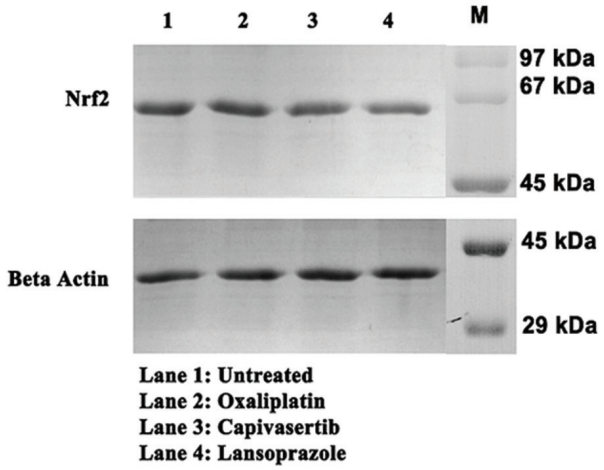

Figure 16. Representative Western blot showing Nrf2 expression in Vero cells treated with selected compounds. Vero cell lysates were analyzed by SDS-PAGE followed by immunoblotting with an anti-Nrf2 antibody. Beta actin was used as the internal loading control. A molecular weight marker (M) indicates bands at 29, 45, 67, and 97 kDa
Abbreviations: Nrf2: Nuclear factor erythroid 2-related factor 2

into the tumor-specific targeting of these compounds, as depicted in Figures 15 and 16.

3.4.4.1. FN3K expression analysis

FN3K expression remained largely unchanged across all treatment groups (Figure 15), with oxaliplatin (1.024) and capivasertib (0.980) showing minimal deviation from the untreated control (0.967). Lansoprazole induced a slight increase in FN3K expression (1.036), representing an approximate 7% upregulation, which is unlikely to have a biologically significant impact. These findings suggest that FN3K-dependent metabolic pathways in normal Vero cells are not strongly affected by these compounds, reinforcing the notion that FN3K inhibition is more relevant in cancer-specific metabolic adaptations.

Comparison with FN3K expression patterns in MCF-7, T-47D, and BT-474 cells reveals that baseline FN3K expression in Vero cells is inherently lower than in cancerous models. This observation supports the hypothesis that FN3K is upregulated in cancer cells as part of metabolic reprogramming, making it a viable tumor-specific target.

3.4.4.2. Nrf2 expression analysis

Nrf2 expression remained relatively stable across all conditions (Figure 16), with only minor variations observed. Oxaliplatin (0.929) led to a slight reduction (~11%), while capivasertib (1.008) and lansoprazole (0.946) showed no significant alterations in expression levels compared to the untreated control (1.049). These findings suggest that the

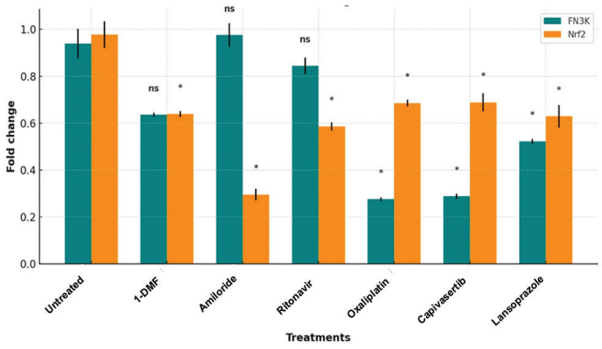

Figure 17. Western blot densitometric analysis of FN3K and Nrf2 expression in MCF-7 cells. Protein expression levels were normalized to beta actin. Welch's t-test with Benjamini-Hochberg correction was applied for statistical analysis. Significant changes ($p<0.05$) are marked with an asterisk (*), while non-significant changes are labeled as ns
Abbreviations: 1-DMF: 1-deoxy-1-morpholino-D-fructose; FN3K: Fructosamine-3-kinase; Nrf2: Nuclear factor erythroid 2-related factor 2

tested compounds do not strongly modulate Nrf2-driven oxidative stress responses in non-cancerous cells.

Notably, Nrf2 expression in untreated Vero cells was already high, indicating strong intrinsic antioxidant defenses typical of normal kidney-derived cells. This aligns with previous findings that non-cancerous epithelial cells rely on robust basal Nrf2 activity to counter oxidative stress, further distinguishing their regulatory mechanisms from those of cancer cells.

3.5. Overall implications

Across all tested breast cancer cell lines, oxaliplatin consistently demonstrated the strongest FN3K inhibition, followed by lansoprazole and capivasertib, with varying degrees of suppression depending on the cell type. The absence of FN3K inhibition in Vero cells confirms that the inhibitory effects observed in MCF-7, T-47D, and BT-474 are cancer-specific rather than the result of generalized cytotoxicity. These findings suggest that FN3K inhibitors preferentially target metabolic pathways in breast cancer cells while sparing normal tissues, highlighting their potential therapeutic relevance.

As this study primarily focused on FN3K inhibition, changes in Nrf2 expression were not a direct objective. According to the proposed mechanism, FN3K inhibition is expected to reduce Nrf2 deglycation, thereby preventing its activation and nuclear translocation. Consequently, Nrf2 expression itself should remain unchanged or show slight upregulation, which is consistent with the observed results. The absence of significant Nrf2 downregulation across all tested cell lines further supports the hypothesis that FN3K inhibition selectively disrupts Nrf2 activation without directly altering its expression levels. These findings

reinforce FN3K as a promising therapeutic target, with minimal impact on oxidative stress regulatory pathways.

3.6. Statistical analysis of FN3K and Nrf2 expression in MCF-7 Cells

Statistical evaluation of FN3K and Nrf2 protein expression across various treatment groups was performed using Welch's t-test, with multiple testing corrections applied through the Benjamini-Hochberg method to control the FDR. Protein levels were normalized against beta actin, and all statistical analyses were carried out using the SciPy and statsmodels libraries in Python. The resulting statistical metrics and significance thresholds are illustrated in Figure 17.

3.6.1. FN3K expression analysis

Oxaliplatin, capivasertib, and lansoprazole significantly downregulated FN3K expression ($p<0.05$), indicating a strong inhibitory effect on this metabolic enzyme (Figure 17). In contrast, 1-DMF ($p=0.060$), amiloride ($p=0.678$), and ritonavir ($p=0.341$) did not significantly alter FN3K expression, suggesting minimal or no impact on this pathway in MCF-7 cells.

3.6.2. Nrf2 expression analysis

All tested compounds, including 1-DMF, amiloride, ritonavir, oxaliplatin, capivasertib, and lansoprazole, significantly suppressed Nrf2 expression ($p<0.05$; Figure 17). This suggests a potential mechanistic link between FN3K inhibition and oxidative stress modulation, reinforcing the idea that these compounds may influence tumor progression through metabolic and redox regulatory pathways.

These findings highlight that oxaliplatin, capivasertib, and lansoprazole effectively target FN3K while also reducing Nrf2 expression. Meanwhile, although 1-DMF, amiloride, and ritonavir did not significantly impact FN3K levels, their ability to suppress Nrf2 suggests possible alternative mechanisms of action related to oxidative stress and redox balance in MCF-7 cells.

3.7. Statistical analysis of FN3K and Nrf2 expression in T-47D Cells

In T-47D cells, statistical analysis of FN3K and Nrf2 protein expression was conducted using Welch's t-test, with FDR correction applied for multiple comparisons. Protein levels were normalized to beta actin, and a p-value below 0.05 was considered statistically significant, as presented in Figure 18.

3.7.1. FN3K expression analysis

Oxaliplatin significantly downregulated FN3K expression ($p=0.048$), suggesting an inhibitory effect on this metabolic enzyme in T-47D cells (Figure 18). In contrast, capivasertib ($p=0.864$) and lansoprazole ($p=0.072$) did not induce statistically significant FN3K suppression, indicating minimal or inconsistent effects on FN3K expression in this cell line.

3.7.2. Nrf2 expression analysis

Nrf2 expression remained largely unaffected across all treatment groups (Figure 18), with oxaliplatin ($p=0.300$), capivasertib ($p=0.657$), and lansoprazole ($p=0.552$) showing no statistically significant changes compared to the untreated control. This suggests that, in T-47D cells, these compounds do not strongly influence oxidative stress regulatory pathways.

These findings highlight a differential regulatory response in T-47D cells compared to MCF-7, where FN3K inhibition was more pronounced and Nrf2 suppression was significant across multiple treatments. The lack of

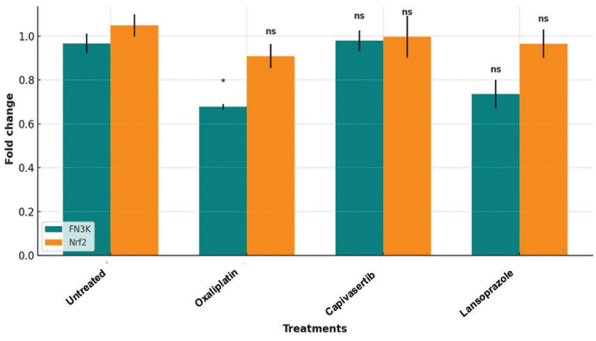

Figure 18. Western blot densitometric analysis of FN3K and Nrf2 expression in T-47D cells. Protein expression levels were normalized to beta actin. Welch's t-test with Benjamini-Hochberg correction was applied. Significant changes ($p<0.05$) are marked with an asterisk (*), while non-significant changes are labeled as ns
Abbreviations: FN3K: Fructosamine-3-kinase; Nrf2: Nuclear factor erythroid 2-related factor 2

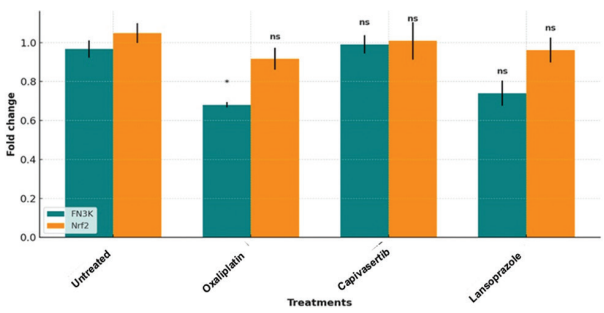

Figure 19. Western blot densitometric analysis of FN3K and Nrf2 expression in BT-474 cells. Protein expression levels were normalized to beta actin. Welch's t-test with Benjamini-Hochberg correction was applied. Significant changes ($p<0.05$) are marked with an asterisk (*), while non-significant changes are labeled as ns
Abbreviations: FN3K: Fructosamine-3-kinase; Nrf2: Nuclear factor erythroid 2-related factor 2

significant Nrf2 modulation in T-47D cells suggests that FN3K suppression in this model may not directly impact oxidative stress signaling, reinforcing the importance of cell-line-specific responses in evaluating potential therapeutic targets.

3.8. Statistical analysis of FN3K and Nrf2 expression in BT-474 Cells

Protein expression changes of FN3K and Nrf2 in BT-474 cells were statistically analyzed using Welch's t-test, with FDR correction applied for multiple testing. Beta actin was used for normalization, and statistical significance was defined as $p<0.05$, as depicted in Figure 19.

3.8.1. FN3K expression analysis

Oxaliplatin induced a marginally significant reduction in FN3K expression ($p=0.049$), suggesting a moderate inhibitory effect on FN3K expression in BT-474 cells (Figure 19). However, capivasertib ($p=0.725$) and lansoprazole ($p=0.077$) did not significantly alter FN3K expression, indicating statistically no significance impact on this pathway in this cell line.

3.8.2. Nrf2 expression analysis

Nrf2 expression remained unchanged across all treatment groups (Figure 19), with oxaliplatin ($p=0.300$), capivasertib ($p=0.739$), and lansoprazole ($p=0.521$) showing no significant differences compared to the untreated control. These results align with trends observed in T-47D cells, where FN3K suppression did not correlate with notable Nrf2 modulation.

These findings suggest that while oxaliplatin exerts a measurable inhibitory effect on FN3K expression in BT-474 cells, capivasertib and lansoprazole do not significantly impact this metabolic enzyme in this context.

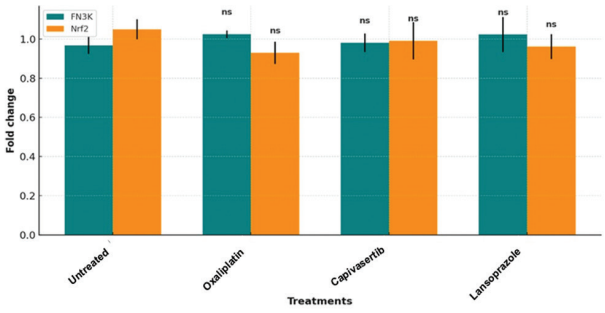

Figure 20: Western blot densitometric analysis of FN3K and Nrf2 expression in Vero cells. Protein expression levels were normalized to beta actin. Welch's t-test with Benjamini-Hochberg correction was applied. No significant changes were observed across treatments, as indicated by the non-significant (ns) labels
Abbreviations: FN3K: Fructosamine-3-kinase; Nrf2: Nuclear factor erythroid 2-related factor 2

In addition, the lack of significant Nrf2 suppression across treatments implies that oxidative stress regulatory pathways in BT-474 cells may be less responsive to these compounds, further reinforcing the importance of considering cell-line-specific variations in therapeutic response.

3.9. Selective FN3K inhibition in cancer: Lack of significant modulation in non-malignant Vero cells

Statistical analysis of Western blot data was performed using Python-based tools, with appropriate tests applied for normality assessment and pairwise comparisons. Multiple comparison correction was implemented to ensure statistical robustness (Figure 20).

3.9.1. FN3K expression analysis

Treatment with oxaliplatin ($p=0.846$), capivasertib ($p=0.846$), and lansoprazole ($p=0.846$) did not result in statistically significant alterations in FN3K expression levels in Vero cells (Figure 20). These results indicate that none of the tested compounds exert an inhibitory effect on FN3K in this non-malignant cell line, further reinforcing the selective suppression of FN3K in cancerous models.

3.9.2. Nrf2 expression analysis

Similarly, Nrf2 expression remained unaffected across all treatment conditions (Figure 20), with oxaliplatin ($p=0.600$), capivasertib ($p=0.624$), and lansoprazole ($p=0.600$) showing no statistically significant changes compared to the untreated control. The absence of Nrf2 modulation suggests that oxidative stress pathways in Vero cells are not significantly influenced by these compounds.

These findings confirm that FN3K inhibition is primarily a cancer-specific event, with minimal impact on non-malignant cell lines, such as Vero cells. The lack of significant FN3K and Nrf2 modulation in these normal cells supports the hypothesis that FN3K suppression occurs preferentially in tumor-specific contexts, reinforcing its potential as a selective therapeutic target in oncology.

3.10. Crosstalk between FN3K and redox-sensitive pathways

While Nrf2 suppression emerged as a consistent downstream effect of FN3K inhibition in our study, we recognize that Nrf2 is a master regulator of cellular redox balance, and its modulation may impact multiple overlapping pathways. FN3K has been shown to deglycate lysine and arginine residues on Nrf2, enhancing its nuclear translocation, sMAF binding, and transcriptional activation of ARE-driven genes, such as *NQO1*, *HO-1*, and *TXNRD1*.[3,10] Our *in vitro* results confirmed FN3K and Nrf2 co-downregulation in breast cancer cells, supporting this mechanistic link. However, Nrf2 activity intersects with a wide array of signaling

cascades – including PI3K/Akt, nuclear factor kappa B (NF-κB), glucose-6-phosphate dehydrogenase (G6PD), hypoxia-inducible factor 1-alpha (HIF1α), and Notch – which govern tumor proliferation, inflammation, and immune evasion.[56,57]

Inhibition of FN3K may thus have pleiotropic effects, not only attenuating Nrf2's antioxidant defense but also disrupting cellular metabolism, mitochondrial function, and DNA repair responses through its deglycation activity on other substrates. FN3K-sensitive proteins include ribosomal subunits, translation factors, histones, and glycolytic enzymes, implying that FN3K may act as a redox-modifying hub beyond Nrf2 stabilization. Moreover, accumulation of AGEs due to reduced FN3K activity can activate RAGE-mediated pathways (PI3K, MAPK, NF-κB), promoting angiogenesis, drug resistance, and cancer progression.[3,10]

While our findings emphasize Nrf2 suppression as a prominent outcome of FN3K inhibition, we acknowledge the possibility of off-target redox modulation. Further pathway-mapping studies are warranted to profile global transcriptional changes, ROS accumulation, and metabolic shifts induced by FN3K inhibition in tumor and normal tissues. These insights will be crucial for identifying synergistic targets and ensuring safety in future pre-clinical development.

3.11. Translational relevance and clinical integration

The repositioning of oxaliplatin, lansoprazole, and capivasertib as FN3K-targeted inhibitors necessitates careful evaluation of their clinical applicability, particularly in breast cancer settings. Oxaliplatin, a third-generation platinum-based chemotherapeutic, has shown efficacy beyond colorectal cancer, including promising results in platinum-pretreated breast and ovarian cancers. Despite dose-limiting peripheral neuropathy, novel strategies, such as chronomodulated delivery and calcium–magnesium infusions have been explored to mitigate toxicity.[53,58,59] Its potential in redox-sensitive tumors supports dose-sparing strategies when used in combination with targeted agents, such as FN3K inhibitors.

Capivasertib, a selective pan-AKT inhibitor, has been validated in hormone receptor-positive and triple-negative breast cancer (TNBC) through trials, such as CAPItello-291, which demonstrated a significant progression-free survival advantage when combined with fulvestrant in patients harboring PI3K/AKT/PTEN alterations. The intermittent 4-days-on/3-days-off (400–480 mg BID) dosing regimen was optimized based on exposure–response modeling to balance efficacy and tolerability, minimizing adverse events like hyperglycemia, rash, and diarrhea.[60] These pharmacological characteristics support its rational inclusion in redox-modulatory and kinase-targeted regimens, including FN3K-focused strategies.

Lansoprazole, traditionally used as a proton pump inhibitor (PPI), has demonstrated potent anti-tumor effects, including HDAC2 inhibition, autophagy modulation, and reversal of drug sequestration in acidic endosomal compartments. Its synergy with chemotherapeutic agents, such as doxorubicin and metronomic cyclophosphamide underscores its capacity to enhance intratumoral drug distribution and overcome microenvironment-induced resistance.[61-64] Importantly, lansoprazole has a wide therapeutic window, favorable oral bioavailability, and a well-established safety profile, making it a viable candidate for combination therapies targeting the FN3K–Nrf2 axis.

Collectively, the clinical readiness of these agents, coupled with their distinct mechanisms of action, offers a pragmatic advantage for rapid translation. Future trials should focus on dose-optimization, toxicity reduction through combination strategies, and patient stratification based on FN3K and Nrf2 expression to ensure precision-guided therapy in breast cancer.

3.12. Statistical limitations and power considerations

Although the experimental results – particularly qPCR and Western blot analyses – revealed statistically significant downregulation of FN3K and Nrf2 across multiple breast cancer cell lines, it is important to acknowledge that this study did not include a formal a priori power analysis. Given the exploratory nature of the study, a fixed number of biological replicates (n = 3 per group) was used, which is consistent with standard practice for preliminary *in vitro* screening studies. Welch's t-test was employed to accommodate unequal variance assumptions, and FDR correction was applied to manage Type I errors in multiple comparisons. However, the small sample size may reduce the power to detect subtle biological effects and increase the risk of false negatives (Type II errors).

Power analysis, which estimates the minimum required sample size to achieve a desired statistical power (commonly 80%) at a defined effect size and significance level (typically $\alpha = 0.05$), is a critical component of confirmatory pre-clinical studies. In this preliminary work, our objective was to identify FN3K-inhibitory candidates and assess differential expression patterns across redox-responsive signaling pathways. The findings from this phase now provide the effect size estimates that will inform formal sample size calculations in subsequent confirmatory studies.

Future validation studies – including *in vivo* tumor xenograft models and expanded *in vitro* assays with dose–response replicates – will incorporate a priori power analyses to optimize statistical robustness, minimize sampling bias, and ensure reproducibility. This stepwise

integration of statistical planning from exploratory to confirmatory phases aligns with best practices in translational cancer research and ensures rigorous evidence generation in subsequent stages of drug development.

3.13. Scope and generalizability of findings

The present study employed three molecularly distinct breast cancer cell lines – MCF-7 (luminal A, ER^+/PR^+), T-47D (luminal B, $ER^+/PR^+/HER2^-$), and BT-474 ($HER2^+$ subtype) – to explore the role of FN3K inhibition across hormone-driven and HER2-amplified breast cancer models. This experimental design was intended to capture a broad segment of the clinical breast cancer spectrum, particularly those subtypes where redox adaptation contributes to treatment resistance.

However, we acknowledge that these models do not encompass the full heterogeneity of breast cancer, especially TNBC, which exhibits distinct redox vulnerabilities and metabolic plasticity. In addition, cancer types outside the breast tissue may exhibit different dependencies on FN3K or Nrf2 signaling, potentially limiting the generalizability of our present findings.

This study was conceptualized as a focused proof-of-concept investigation into the feasibility of repurposing FN3K-targeted agents in selected breast cancer subtypes. Moving forward, we aim to expand our experimental scope by incorporating TNBC cell lines and non-breast cancer models with known oxidative stress signatures, such as lung, liver, and pancreatic cancers. These comparative studies will enable systematic mapping of FN3K expression, redox pathway activation, and drug responsiveness across cancer types.

4. Molecular dynamics (MD) simulations of lead molecules

Following *in vitro* confirmation of FN3K inhibition by lansoprazole, capivasertib, and oxaliplatin, MD simulations were employed to gain deeper insight into their binding stability, conformational behavior, and key molecular interactions within the FN3K active site. Simulations were conducted using Desmond version 13.7 (Schrödinger, LLC, USA) with the OPLS5 force field, placing the complexes in an orthorhombic simulation box solvated with TIP3P water molecules. The system was initially energy-minimized and subsequently equilibrated under NPT ensemble conditions at 300 K and 1 atm pressure. A production simulation was carried out for 200 ns with a 2-femtosecond timestep, applying the Particle Mesh Ewald (PME) method for long-range electrostatics and a 9 Å cutoff for van der Waals interactions. Post-simulation trajectory analyses – including root mean square deviation (RMSD), root mean square fluctuation (RMSF), radius of gyration (rGyr), and hydrogen bond occupancy – were performed to evaluate complex stability and dynamic binding features, offering comprehensive insights into the affinity and interaction profiles of the selected lead compounds.[65]

4.1. Selection of lead molecules for MD simulations

The selection of lansoprazole, capivasertib, and oxaliplatin for MD simulations was based on three primary criteria. First, all three compounds demonstrated strong FN3K inhibition, with reductions ranging from 99.6% to 99.99% across multiple breast cancer cell lines (MCF-7, T-47D, BT-474). Second, these compounds exhibited minimal off-target effects in non-malignant Vero cells, reinforcing their tumor-selective properties. Finally, their favorable ADMET profiles further supported their candidacy: Capivasertib and lansoprazole showed high gastrointestinal absorption, while oxaliplatin demonstrated high solubility, making all three suitable for further evaluation through MD simulations.

4.2. Objective of MD simulations

To investigate the molecular interactions and dynamic stability of the lead candidates – lansoprazole, capivasertib, and oxaliplatin – in complex with FN3K, MD simulations were conducted for 200 ns using Desmond. Several key parameters were evaluated to characterize the behavior and binding profiles of the complexes. RMSD was employed to monitor the overall structural stability of the protein-ligand complex throughout the simulation, while RMSF assessed the flexibility and mobility of amino acid residues, particularly within the active site, in response to ligand binding. Hydrogen bond analysis was performed to examine the consistency and strength of hydrogen bonding interactions between the ligand and FN3K over the simulation trajectory. In addition, binding free energy was calculated using MM-GBSA or MM-PBSA methods to estimate the thermodynamic favorability and strength of binding for each compound. Finally, total energy calculations were conducted within Desmond to analyze the system's potential and interaction energies, offering insights into conformational stability and favorable binding orientations.

Findings from the MD simulations offer valuable mechanistic insights into FN3K inhibition, supporting the therapeutic relevance of the identified lead compounds. The full simulation trajectories and detailed parameter-specific results – such as RMSD, RMSF, rGyr, hydrogen bonding, and MM-GBSA binding energy analyses – are presented in Supplementary Figures S7-S40.

5. Future perspectives

The findings of this study provide a strong foundation for exploring FN3K inhibition as a novel therapeutic strategy

for breast cancer. However, several critical avenues remain to be explored to fully establish its clinical relevance. First, while the study establishes the inhibitory effects of selected FN3K inhibitors on breast cancer cell lines, further in-depth mechanistic investigations are required to elucidate the precise molecular role of FN3K in cancer progression. These should include studies on FN3K-mediated metabolic adaptations and its impact on oxidative stress pathways beyond Nrf2 signaling; as such investigations would provide deeper insights into its therapeutic potential. Secondly, *in vivo* studies and pharmacokinetics are critical; although initial *in vivo* validation demonstrated significant tumor growth suppression, comprehensive pharmacokinetic and toxicological evaluations in animal models are essential. Determining the bioavailability, metabolic stability, and potential off-target effects of FN3K inhibitors will be crucial before progressing to clinical trials. In addition, the development of selective FN3K inhibitors from existing FDA-approved drugs, future efforts should focus on rational drug design to develop more selective inhibitors with minimal off-target effects. Computational approaches, such as MD simulations and free energy perturbation studies can aid in optimizing lead compounds for enhanced specificity and efficacy. Furthermore, exploration of combination therapies is warranted. Given the role of FN3K in modulating oxidative stress responses, investigating its inhibition in combination with chemotherapeutic agents or targeted therapies could provide synergistic effects. Evaluating the impact of FN3K inhibitors on drug resistance mechanisms may reveal novel combination strategies to enhance treatment efficacy. For clinical translation and biomarker development, studies should assess FN3K expression patterns in patient-derived tumor samples and correlate them with disease progression and treatment response. Identifying reliable biomarkers associated with FN3K inhibition will be instrumental in patient stratification and personalized therapy approaches. Finally, CRISPR/Cas9-based gene editing approaches, including knockout or knockdown studies in breast cancer models, can help validate the direct contribution of FN3K to tumorigenesis. Functional studies in FN3K-deficient models will clarify its essentiality in breast cancer survival and progression.

By addressing these critical aspects, FN3K-targeted therapy can move closer to clinical application, offering a promising avenue for breast cancer treatment.

6. Conclusion

The present study underscores the therapeutic potential of targeting FN3K in breast cancer management. By integrating *in silico* virtual screening with *in vitro* validation, we identified lead compounds – oxaliplatin, lansoprazole, and capivasertib – that significantly inhibited FN3K expression and function. This inhibition was corresponded with suppression of Nrf2-mediated antioxidant signaling and reduced cancer cell viability, supporting the role of FN3K in tumor progression and redox adaptation.

Importantly, all three compounds demonstrated strong selectivity toward breast cancer cells with minimal cytotoxicity in normal cells, indicating a favorable therapeutic index. These findings collectively support the FN3K–Nrf2 axis as a promising molecular target in redox-driven breast cancer subtypes.

While the present findings are encouraging, we acknowledge the limitation that *in vivo* validation was not included in this phase of the study. To address this, future experiments are already planned to assess the efficacy and safety of FN3K inhibition in xenograft tumor models. These will include evaluation of tumor growth suppression, pharmacokinetic profiles, and modulation of the FN3K–Nrf2 axis in excised tumor tissues. In addition, downstream molecular pathway mapping, ADME optimization, and combinatorial strategies with standard therapeutics will be explored to facilitate translational relevance.

Overall, this work establishes FN3K inhibition as a viable therapeutic strategy for breast cancer and provides a strong foundation for future *in vivo* and clinical investigations. Based on the present stage of validation, oxaliplatin, lansoprazole, and capivasertib should be regarded as promising pre-clinical candidates for FN3K-targeted intervention, rather than as definitive therapeutic options. Further *in vivo* and combination therapy studies are required to fully determine their clinical applicability.

Acknowledgments

The authors acknowledge the JSS Academy of Higher Education and Research and the JSS College of Pharmacy for providing institutional support. The Department of Computer Aided Drug Design is gratefully acknowledged for providing the computational resources essential for the *in silico* studies. The authors also express their sincere thanks to Dr. Subramanyam P, Muppandal Genomics and Immunologicals Pvt. Ltd., Hyderabad, for his technical assistance in conducting the *in vitro* biological experiments and supporting data validation.

Funding

The work was supported by the Council of Scientific and Industrial Research, Human Resource Development Group (CSIR-HRDG), New Delhi, India (Grant No.111-5634- 11759/2023/1 dated February 19th, 2024).

Conflict of interest

The authors have no relevant financial or non-financial interests to disclose.

Author contributions

Conceptualization: Gurupadayya Bannimath, Prabitha Prabhakaran
Data curation: Erica Alves
Formal analysis: Erica Alves, Prabitha Prabhakaran
Investigation: Erica Alves
Methodology: Erica Alves
Software: Erica Alves
Validation: Erica Alves, Prabitha Prabhakaran
Writing – original draft: Erica Alves
Writing – review & editing: Erica Alves

Ethics approval and consent to participate

Not applicable.

Consent for publication

Not applicable.

Availability of data

All data generated or analyzed during this study are included in this published article and its supplementary files, which can be accessed in https://docs.google.com/document/d/1KTlZzQXsTetJk5wVh7Hyw6cdw6UK0HRl/edit?usp=sharing&ouid=103717361144569370602&rtpof=true&sd=true Additional datasets supporting the findings of this study are available from the corresponding author upon reasonable request.

References

1. Tufail M, Jiang CH, Li N. Altered metabolism in cancer: Insights into energy pathways and therapeutic targets. *Mol Cancer.* 2024;23(1):203.

   doi: 10.1186/s12943-024-02119-3

2. Yousefi T, Pasha ARG, Kamrani G, *et al.* Evaluation of fructosamine 3-kinase and glyoxalase 1 activity in normal and breast cancer tissues. *Biomedicine (Taipei).* 2021;11(3):15-22.

   doi: 10.37796/2211-8039.1130

3. Alves E, Bannimath G, Prabhakaran P, Beeraka NM. The FN3K-Nrf2 axis: A novel therapeutic target in cancer metabolism. *Eurasian J Med Oncol.* 2024;8(4):338-339.

   doi: 10.14744/ejmo.2024.20665

4. Sanghvi VR, Leibold J, Mina M, *et al.* The oncogenic action of NRF2 depends on de-glycation by fructosamine-3-kinase. *Cell.* 2019;178(4):807-819.e21.

   doi: 10.1016/j.cell.2019.07.031

5. Beeraka NM, Zhang J, Mandal S, *et al.* Screening fructosamine-3-kinase (FN3K) inhibitors, a deglycating enzyme of oncogenic Nrf2: Human FN3K homology modelling, docking and molecular dynamics simulations. *PLoS One.* 2023;18(11):e0283705.

   doi: 10.1371/journal.pone.0283705

6. Beeraka NM, Zhang J, Uthaiah CA, *et al.* Expression patterns and relevance of FN3K, Nrf2, and NQO1 in breast cancers. *Eurasian J Med Oncol.* 2024;8(1):88-105.

   doi: 10.14744/ejmo.2024.61033

7. Delpierre G, Collard F, Fortpied J, Van Schaftingen E. Fructosamine 3-kinase, an enzyme involved in protein deglycation. *Biochem Soc Trans.* 2004;32(6):813-816.

   doi: 10.1042/bst0320813

8. Lionta E, Spyrou G, Vassilatis DK, Cournia Z. Structure-based virtual screening for drug discovery: Principles, applications and recent advances. *Curr Top Med Chem.* 2014;14(16):1923-1938.

   doi: 10.2174/1568026614666140929124445

9. Roskoski R Jr. Properties of FDA-approved small molecule protein kinase inhibitors: A 2023 update. *Pharmacol Res.* 2023;187:106552.

   doi: 10.1016/j.phrs.2023.106552

10. Beeraka NM, Bovilla VR, Doreswamy SH, Puttalingaiah S, Srinivasan A, Madhunapantula SV. The taming of nuclear factor erythroid-2-related factor-2 (Nrf2) deglycation by fructosamine-3-kinase (FN3K)-inhibitors-a novel strategy to combat cancers. *Cancers (Basel).* 2021;13(2):281.

    doi: 10.3390/cancers13020281

11. Beeraka NM, Zhang J, Zhao D, *et al.* Combinatorial implications of Nrf2 inhibitors with FN3K inhibitor: *In vitro* breast cancer study. *Curr Pharm Des.* 2023;29(30):2408-2425.

    doi: 10.2174/0113816128261466231011114600

12. Carles F, Bourg S, Meyer C, Bonnet P. PKIDB: A curated, annotated and updated database of protein kinase inhibitors in clinical trials. *Molecules.* 2018;23(4):908.

    doi: 10.3390/molecules23040908

13. World Health Organization. *WHO Model Lists of Essential Medicines. 23rd List*; 2023. Available from: https://www.who.int/publications/i/item/WHO-MHP-HPS-EML-2023.01 [Last accessed on 2025 Mar 14].

14. National Cancer Institute. *Breast Cancer Treatment Drugs*. Bethesda, MD: National Cancer Institute. Available from: https://www.cancer.gov/about-cancer/treatment/drugs/breast [Last accessed on 2025 Mar 14].

15. Cheng T, Li Q, Zhou Z, Wang Y, Bryant SH. Structure-based virtual screening for drug discovery: A problem-centric review. *AAPS J.* 2012;14(1):133-141.

doi: 10.1208/s12248-012-9322-0

16. Hevener KE, Pesavento R, Ren J, Lee H, Ratia K, Johnson ME. Hit-to-lead: Hit validation and assessment. *Methods Enzymol.* 2018;610:265-309.

doi: 10.1016/bs.mie.2018.09.022

17. Wang XJ, Sun Z, Villeneuve NF, *et al.* Nrf2 enhances resistance of cancer cells to chemotherapeutic drugs, the dark side of Nrf2. *Carcinogenesis.* 2008;29(6):1235-1243.

doi: 10.1093/carcin/bgn095

18. Schrödinger LLC. *Maestro: Schrödinger Release 2024-1*. New York, NY: Schrödinger, LLC; 2024. Available from: https://www.schrodinger.com/maestro [Last accessed on 2025 Feb 21].

19. Friesner RA, Murphy RB, Repasky MP, *et al.* Extra precision glide: Docking and scoring incorporating a model of hydrophobic enclosure for protein-ligand complexes. *J Med Chem.* 2006;49(21):6177-6196.

doi: 10.1021/jm051256o

20. Liu T, Lu D, Zhang H, *et al.* Applying high-performance computing in drug discovery and molecular simulation. *Natl Sci Rev.* 2016;3(1):49-63.

doi: 10.1093/nsr/nww003

21. UniProt Consortium. UniProt: A worldwide hub of protein knowledge. *Nucleic Acids Res.* 2019;47(D1):D506-D515.

doi: 10.1093/nar/gky1049

22. UniProt. *FN3K Fructosamine-3-Kinase Homo Sapiens (Human)*. UniProtKB; 2025. Available from: https://www.uniprot.org/uniprotkb/q9H479/entry [Last accessed on 2025 Mar 15].

23. Sievers F, Higgins DG. Clustal Omega for making accurate alignments of many protein sequences. *Protein Sci.* 2018;27(1):135-145.

doi: 10.1002/pro.3290

24. Schwede T, Kopp J, Guex N, Peitsch MC. SWISS-MODEL: An automated protein homology-modeling server. *Nucleic Acids Res.* 2003;31(13):3381-3385.

doi: 10.1093/nar/gkg520

25. Ko J, Park H, Heo L, Seok C. GalaxyWEB server for protein structure prediction and refinement. *Nucleic Acids Res.* 2012;40(Web Server issue):W294-W297.

doi: 10.1093/nar/gks493

26. Kleywegt GJ, Jones TA. Phi/Psi-chology: Ramachandran revisited. *Structure.* 1996;4(12):1395-1400.

doi: 10.1016/S0969-2126(96)00147-5

27. University of California, Los Angeles (UCLA). *SAVES - Structure Analysis and Verification Server*. Available from: https://saves.mbi.ucla.edu [Last accessed on 2025 Mar 15].

28. Biasini M, Bienert S, Waterhouse A, *et al.* SWISS-MODEL: Modelling protein tertiary and quaternary structure using evolutionary information. *Nucleic Acids Res.* 2014;42(Web Server issue):W252-W258.

doi: 10.1093/nar/gku340

29. Benkert P, Tosatto SC, Schomburg D. QMEAN: A comprehensive scoring function for model quality assessment. *Proteins.* 2008;71(1):261-277.

doi: 10.1002/prot.21715

30. Benkert P, Biasini M, Schwede T. Toward the estimation of the absolute quality of individual protein structure models. *Bioinformatics.* 2011;27(3):343-350.

doi: 10.1093/bioinformatics/btq662

31. Schrödinger LLC. *Protein Preparation Workflow*. Schrödinger. Available from: https://www.schrodinger.com/life-science/learn/white-papers/protein-preparation-workflow [Last accessed on 2025 Mar 15].

32. National Center for Biotechnology Information (NCBI). PubChem. Available from: https://pubchem.ncbi.nlm.nih.gov [Last accessed on 2025 Mar 15].

33. Knox C, Wilson M, Klinger CM, *et al.* DrugBank 6.0: The drugbank knowledgebase for 2024. *Nucleic Acids Res.* 2024;52(D1):D1265-D1275.

doi: 10.1093/nar/gkad976

34. Sahayarayan JJ, Rajan KS, Vidhyavathi R, *et al. In-silico* protein-ligand docking studies against the estrogen protein of breast cancer using pharmacophore based virtual screening approaches. *Saudi J Biol Sci.* 2021;28(1):400-407.

doi: 10.1016/j.sjbs.2020.10.023

35. Ge Y, Pande V, Seierstad MJ, Damm-Ganamet KL. Exploring the application of sitemap and site finder for focused cryptic pocket identification. *J Phys Chem B.* 2024;128(26):6233-6245.

doi: 10.1021/acs.jpcb.4c00664

36. Elekofehinti OO, Iwaloye O, Josiah SS, Lawal AO, Akinjiyan MO, Ariyo EO. Molecular docking studies, molecular dynamics and ADME/tox reveal therapeutic potentials of STOCK1N-69160 against papain-like protease of SARS-CoV-2. *Mol Divers.* 2021;25:1761-1773.

doi: 10.1007/s11030-020-10151-w

37. Park MS, Dessal AL, Smrcka AV, Stern HA. Evaluating docking methods for prediction of binding affinities of small molecules to the G protein betagamma subunits. *J Chem Inf Model.* 2010;49(2):437-443.

doi: 10.1021/ci800412z

38. Daina A, Michielin O, Zoete V. SwissADME: A free web tool to evaluate pharmacokinetics, drug-likeness and medicinal chemistry friendliness of small molecules. *Sci Rep.* 2017;7:42717.

doi: 10.1038/srep42717

39. Li W, Zhou J, Xu Y. Study of the *in vitro* cytotoxicity testing of medical devices. *Biomed Rep.* 2015;3(5):617-620.

doi: 10.3892/br.2015.481

40. International Organization for Standardization. *ISO 10993-5:2009. Biological Evaluation of Medical Devices-Part 5: Tests for In Vitro Cytotoxicity.* 3rd ed. Geneva: ISO; 2009.

41. Senthilraja P, Kathiresan K. *In vitro* cytotoxicity MTT assay in vero, HepG2 and MCF-7 cell lines study of marine yeast. *J Appl Pharm Sci.* 2015;5(3):80-84.

doi: 10.7324/JAPS.2015.50313

42. Freshney RI. *Culture of Animal Cells: A Manual of Basic Technique and Specialized Applications.* 6th ed. Hoboken, NJ: Wiley-Blackwell; 2010.

43. Chomczynski P, Sacchi N. Single-step method of RNA isolation by acid guanidinium thiocyanate-phenol-chloroform extraction. *Anal Biochem.* 1987;162(1):156-159.

doi: 10.1016/0003-2697(87)90021-2

44. Rio DC, Ares M Jr., Hannon GJ, Nilsen TW. Determining the yield and quality of purified RNA. *Cold Spring Harb Protoc.* 2010;2010(6).

doi: 10.1101/pdb.top82

45. Taylor SC, Laperriere G, Germain H. Droplet digital PCR versus qPCR for gene expression analysis with low abundant targets: From variable nonsense to publication quality data. *Sci Rep.* 2017;7(1):2409.

doi: 10.1038/s41598-017-02217-x

46. Livak KJ, Schmittgen TD. Analysis of relative gene expression data using real-time quantitative PCR and the 2−ΔΔCt method. *Methods.* 2001;25(4):402-408.

doi: 10.1006/meth.2001.1262

47. Pfaffl MW. A new mathematical model for relative quantification in real-time RT-PCR. *Nucleic Acids Res.* 2001;29(9):e45.

doi: 10.1093/nar/29.9.e45

48. Mahmood T, Yang PC. Western blot: Technique, theory, and trouble shooting. *N Am J Med Sci.* 2012;4(9):429-434.

doi: 10.4103/1947-2714.100998

49. Taylor SC, Posch A. The design of a quantitative western blot experiment. *Biomed Res Int.* 2014;2014:361590.

doi: 10.1155/2014/361590

50. Virtanen P, Gommers R, Oliphant TE, *et al.* SciPy 1.0: Fundamental algorithms for scientific computing in python. *Nat Methods.* 2020;17(3):261-272.

doi: 10.1038/s41592-019-0686-2

51. Ahad NA, Syed Yahaya SS. Sensitivity analysis of Welch's t-test. *AIP Conf Proc.* 2014;1605:888-893.

doi: 10.1063/1.4887707

52. Lee S, Lee DK. What is the proper way to apply the multiple comparison test. *Korean J Anesthesiol.* 2018;71(5):353-360.

doi: 10.4097/kja.d.18.00242

53. Kasi A. Oxaliplatin. In: *StatPearls*. Treasure Island, FL: StatPearls Publishing; 2025. Available from: https://www.ncbi.nlm.nih.gov/books/nbk557690 [Last accessed on 2023 May 16].

54. Fernandez-Teruel C, Cullberg M, González-García I, Schiavon G, Zhou D. An exposure-safety analysis to support the dosage of the novel AKT inhibitor capivasertib. *Cancer Chemother Pharmacol.* 2025;95:48.

doi: 10.1007/s00280-025-04775-8

55. Ahmed A, Clarke JO. Proton Pump Inhibitors (PPI). In: *StatPearls*. Treasure Island, FL: StatPearls Publishing; 2025. Available from: https://www.ncbi.nlm.nih.gov/books/nbk557385 [Last accessed on 2023 May 01].

56. Lau A, Villeneuve NF, Sun Z, Wong PK, Zhang DD. Dual roles of Nrf2 in cancer. *Pharmacol Res.* 2008;58(5-6):262-270.

doi: 10.1016/j.phrs.2008.09.003

57. Kumar H, Kumar RM, Bhattacharjee D, Somanna P, Jain V. Role of Nrf2 signaling cascade in breast cancer: Strategies and treatment. *Front Pharmacol.* 2022;13:720076.

doi: 10.3389/fphar.2022.720076

58. Bogliolo S, Cassani C, Gardella B, *et al.* Oxaliplatin for the treatment of ovarian cancer. *Expert Opin Investig Drugs.* 2015;24(9):1275-1286.

doi: 10.1517/13543784.2015.1062874

59. Innominato PF, Karaboué A, Focan C, *et al.* Efficacy and safety of chronomodulated irinotecan, oxaliplatin, 5-fluorouracil and leucovorin combination as first- or second-line treatment against metastatic colorectal cancer: Results from the international EORTC 05011 trial. *Int J Cancer.* 2021;148(10):2512-2521.

doi: 10.1002/ijc.33422

60. Rugo HS, Oliveira M, Howell SJ, *et al.* Capivasertib and fulvestrant for patients with hormone receptor-positive advanced breast cancer: Characterization, time course, and management of frequent adverse events from the phase III CAPItello-291 study. *ESMO Open.* 2024;9(9):103697.

doi: 10.1016/j.esmoop.2024.103697

61. Khadempar S, Lotfi M, Haghiralsadat F, Saidijam M, Ghasemi N, Afshar S. Lansoprazole as a potent HDAC2 inhibitor for treatment of colorectal cancer: An *in-silico* analysis and experimental validation. *Comput Biol Med.* 2023;166:107518.

doi: 10.1016/j.compbiomed.2023.107518

62. Spugnini EP, Buglioni S, Carocci F, *et al.* High dose lansoprazole combined with metronomic chemotherapy: A phase I/II study in companion animals with spontaneously occurring tumors. *J Transl Med.* 2014;12:225.

doi: 10.1186/s12967-014-0225-y

63. Fais S, De Milito A, You H, Qin W. Targeting vacuolar H^+-ATPases as a new strategy against cancer. *Cancer Res.* 2007;67(22):10627-10630.

doi: 10.1158/0008-5472.CAN-07-1805

64. Kao HW, Tsai KW, Lin WC. Synergistic effect of metformin and lansoprazole against gastric cancer through growth inhibition. *Int J Med Sci.* 2023;20(6):717-724.

doi: 10.7150/ijms.82407

65. Salo-Ahen OMH, Alanko I, Bhadane R, *et al.* Molecular dynamics simulations in drug discovery and pharmaceutical development. *Processes.* 2021;9(1):71.

doi: 10.3390/pr9010071